arXiv:1409.1764v5 [math.GT] 13 Jan 2016

Quandle theory and the optimistic limits of the representations of link groups

Jinseok Cho

January 14, 2016

Abstract

When a boudnary-parabolic representation of a link group to PSL(2,$\mathbb{C}$) is given, Inoue and Kabaya suggested a combinatorial method to obtain the developing map of the representation using the octahedral triangulation and the shadow-coloring of certain quandle. Quandle is an algebraic system closely related with the Reidemeister moves, so their method changes quite naturally under the Reidemeister moves.

In this article, we apply their method to the potential function, which was used to define the optimsitic limit, and construct a saddle point of the function. This construction works for any boundary-parabolic representation, and it shows that the octahedral triangulation is good enough to study all possible boundary-parabolic representations of the link group. Furthermore the evaluation of the potential function at the saddle point becomes the complex volume of the representation, and this saddle point changes naturally under the Reidemeister moves because it is constructed using the quandle.

1 Introduction

A link L has the hyperbolic structure when there exists a discrete faithful representation $\rho : \pi_1(L) \to \mathrm{PSL}(2, \mathbb{C})$, where *the link group* $\pi_1(L)$ is the fundamental group of the link complement $\mathbb{S}^3 \backslash L$. The standard method to find the hyperbolic structure of L is to consider some triangulation of $\mathbb{S}^3 \backslash L$ and solve certain set of equations. (These equations are called *the hyperbolicity equations*.) Each solution determines a boundary-parabolic representation[1] and one of them is *the geometric representation*, which means the determined boundary-parabolic representation is discrete and faithful. Due to Mostow's rigidity theorem, the hyperbolic structure of a link is a topological property. Therefore, the invariance of the hyperbolic structure under the Reidemeister moves should be observed. However, this could not be seen easily because, even small alteration on the triangulation changes the solution radically.

[1] *Boundary-parabolic* means the image of the peripheral subgroup $\pi_1(\partial(\mathbb{S}^3 \backslash L))$ is a parabolic subgroup of PSL(2, $\mathbb{C}$). Note that the geometric representation is boundary-parabolic.

Recently, Inoue and Kabaya, in [9], developed a method to construct the hyperbolic structure of L using the link diagram and the geometric representation. More generally, when a boundary-parabolic representation ρ is given, they constructed the explicit geometric shapes of the tetrahedra of certain triangulation using ρ. Their main method is to construct the geometric shapes using certain quandle homology, which is defined directly from the link diagram D and the representation ρ. Here, quandle is an algebric system whose axioms are closely related with the Reidemeister moves of link diagrams, so their construction changes quite naturally under the Reidemeister moves. (The definition of the quandle is in Section 2.1. A good survey of quandle is the book [6].) Therefore the article [9] actually suggested a combinatorial method to obtain the hyperbolic structure of the link complement.

Interestingly, the triangulation they used in [9] was also used to define the optimistic limit of the Kashaev invariant at [4]. As a matter of fact, this triangulation arises naturally from the link diagram. (See Section 3 of [14] and Section 2.3 of this article for the definition.) We call this triangulation *octahedral triangulation* of $\mathbb{S}^3\backslash(L \cup \{\text{two points}\})$ associated with the link diagram D.

The optimistic limit was first appeared in [10] when Kashaev proposed the volume conjecture. This conjecture relates certain limits of link invariants, called Kashaev invariants, with the hyperbolic volumes. The optimistic limit is the value of certain potential function evaluated at a saddle point, where the function and the value are expected to be an analytic continuation of the Kashaev invariant and the limit of the invariant, respectively. As a matter of fact, physicists usually call the evaluation *the classical limit* and consider it *the actual limit* of the invariant. The author and several others developed several versions of the optimistic limit in many articles, but we will modify the version of [4] in this article because this is based on a natural definition.

The optimistic limit is defined by the potential function $V(z_1, \ldots, z_n, w_k^j, \ldots)$. Previously, in [4], this function was defined purely by the link diagram, but here we modify it using the information of the representation ρ. (The definition is in Section 3.) We consider a solution of the following set

$$\mathcal{H} := \left\{ \exp(z_k \frac{\partial V}{\partial z_k}) = 1, \ \ \exp(w_k^j \frac{\partial V}{\partial w_k^j}) = 1 \,\middle|\, j : \text{degenerate}, \ k = 1, \ldots, n \right\},$$

which is a saddle-point of the potential function V. Then Proposition 3.1 will show that $\mathcal{H}$ becomes the hyperbolicity equations of the octahedral triangulation. Furthermore, we will construct an explicit solution $(z_1^{(0)}, \ldots, z_n^{(0)}, (w_k^j)^{(0)}, \ldots)$ of $\mathcal{H}$ by using the quandle associated with the representation ρ. (The exact formulas are in Theorem 3.2.) After defining

$$\begin{aligned} V_0(z_1, \ldots, z_n, (w_k^j), \ldots) &:= V(z_1, \ldots, z_n, (w_k^j), \ldots) \\ &- \sum_k \left(z_k \frac{\partial V}{\partial z_k} \right) \log z_k - \sum_{\substack{j:\text{degenerate} \\ k}} \left(w_k^j \frac{\partial V}{\partial w_k^j} \right) \log w_k^j, \end{aligned}$$

we will show

$$V_0(z_1^{(0)}, \ldots, z_n^{(0)}, (w_k^j)^{(0)}, \ldots) \equiv i(\mathrm{vol}(\rho) + i\,\mathrm{cs}(\rho)) \pmod{\pi^2} \tag{1}$$

at Theorem 3.3, where $\mathrm{vol}(\rho)$ and $\mathrm{cs}(\rho)$ are the hyperbolic volume and the Chern-Simons invariant of ρ defined in [15], respectively. The left-hand side of (1) is called *the optimistic limit of* ρ, and $\mathrm{vol}(\rho) + i\,\mathrm{cs}(\rho)$ in the right-hand side is called *the complex volume of* ρ.

Note that for any boundary-parabolic representation ρ, we can always construct the solution associated with ρ. This implies that the octahedral triangulation is good enough for the study of all possible boundary-parabolic representations from the link group to $\mathrm{PSL}(2,\mathbb{C})$. The set of all possible representations can be regarded as *the Ptolemy variety* (see [7] for detail) and we expect the octahedral triangulation will be very useful to the study of the Ptolemy variety. (Actual application to the Ptolemy variety is in preparation now.)

Furthermore, the construction of the solution is based on the quandle in [9]. Therefore, this solution changes locally under the Reidemeister moves. This implies that we can explore the hyperbolic structure of a link by finding the solution and keeping track of the changes of the solution under the Reidemeister moves. As a matter of fact, after the appearance of the first draft of this article, this idea turned out to be very useful. (Note that this is the second and the final draft.) The author found many interesting applications of this idea at [2], [3] and [5], and some more are in preparation now.

Among the applications, we remark that the article [2] contains very similar results with this article. Both articles construct the solution associated with ρ using the same quandle. However, the major differences are the triangulations. Both uses the same *octahedral decomposition* of $\mathbb{S}^3\backslash(L \cup \{\text{two points}\})$, but this article uses the subdivision of each octahedron into four tetrahedra and call the result *four-term (or octahedral) triangulation*, whereas the article [2] uses the subdivision of the same octahedron into five tetrahedra and call the result *five-term triangulation*. Some tetrahedron in the four-term triangulation can be degenerate and this incurs technical difficulties. However, the five-term triangulation used in [2] does not contain any degenerate tetrahedron, so it is far easier and convenient. (That is why this article is three times longer than [2].) As a conclusion, this article contains the original idea of using quandle to construct the solution and the article [2] improved this idea.

This article consists of the following contents. In Section 2, we will summarize some results of [9]. Especially, the definition of the quandle and the octahedral triangulation will appear. Section 3 will define the optimistic limit and the hyperbolicity equations. The main formula (Theorem 3.3) of the solution associated with the given representation ρ will appear. Section 4 will discuss two simple examples, the figure-eight knot 4_1 and the trefoil knot 3_1.

2 Quandle

In this section, we will survey some results of the article [9]. We remark that all formulas of this section come from [9] and the author learned them from the series lectures of Ayumu Inoue given at Seoul National University during spring of 2012.

2.1 Conjugation quandle of parabolic elements

Definition 2.1. *A **quandle** is a set X with a binary operation $*$ satisfying the following three conditions:*

1. *$a * a = a$ for any $a \in X$,*
2. *the map $*b : X \to X$ $(a \mapsto a * b)$ is bijective for any $b \in X$,*
3. *$(a * b) * c = (a * c) * (b * c)$ for any $a, b, c \in X$.*

The inverse of $*b$ is notated by $*^{-1}b$. In other words, the equation $a *^{-1} b = c$ is equivalent to $c * b = a$.

Definition 2.2. *Let G be a group and X be a subset of G satisfying*

$$gXg^{-1} = X \text{ for any } g \in G.$$

Define the binary operation $*$ on X by

$$a * b = bab^{-1} \tag{2}$$

*for any $a, b \in X$. Then $(X, *)$ becomes a quandle and is called the **conjugation quandle**.*

As an example, let $\mathcal{P}$ be the set of parabolic elements of $\mathrm{PSL}(2, \mathbb{C}) = \mathrm{Isom}^+(\mathbb{H}^3)$. Then

$$g\mathcal{P}g^{-1} = \mathcal{P}$$

holds for any $g \in \mathrm{PSL}(2, \mathbb{C})$. Therefore, $(\mathcal{P}, *)$ is a conjugation quandle, and this is the only quandle we are using in this article.

To perform concrete calculations, explicit expression of $(\mathcal{P}, *)$ was introduced at [9]. At first, note that

$$\begin{pmatrix} p & q \\ r & s \end{pmatrix}^{-1} \begin{pmatrix} 1 & 1 \\ 0 & 1 \end{pmatrix} \begin{pmatrix} p & q \\ r & s \end{pmatrix} = \begin{pmatrix} 1 + rs & s^2 \\ -r^2 & 1 - rs \end{pmatrix},$$

for $\begin{pmatrix} p & q \\ r & s \end{pmatrix} \in \mathrm{PSL}(2, \mathbb{C})$. Therefore, we can identify $(\mathbb{C}^2 \backslash \{0\})/\pm$ with $\mathcal{P}$ by

$$\begin{pmatrix} \alpha & \beta \end{pmatrix} \longleftrightarrow \begin{pmatrix} 1 + \alpha\beta & \beta^2 \\ -\alpha^2 & 1 - \alpha\beta \end{pmatrix}, \tag{3}$$

where $\pm$ means the equivalence relation $\begin{pmatrix} \alpha & \beta \end{pmatrix} \sim \begin{pmatrix} -\alpha & -\beta \end{pmatrix}$. To use the left-side action of $\mathrm{PSL}(2, \mathbb{C})$ on $(\mathbb{C}^2 \backslash \{0\})/\pm$, we consider the transpose of (3) by

$$\begin{pmatrix} \alpha \\ \beta \end{pmatrix} \longleftrightarrow \begin{pmatrix} 1 + \alpha\beta & -\alpha^2 \\ \beta^2 & 1 - \alpha\beta \end{pmatrix},$$

and define the operation $*$ by

$$\begin{pmatrix} \alpha \\ \beta \end{pmatrix} * \begin{pmatrix} \gamma \\ \delta \end{pmatrix} := \begin{pmatrix} 1+\gamma\delta & -\gamma^2 \\ \delta^2 & 1-\gamma\delta \end{pmatrix} \begin{pmatrix} \alpha \\ \beta \end{pmatrix} \in (\mathbb{C}^2\backslash\{0\})/\pm,$$

where the matrix multiplication on the right-hand side is the standard multiplication. Note that this definition coincides with the operation of the conjugation quandle $(\mathcal{P}, *)$ by

$$\begin{aligned} \begin{pmatrix} \alpha \\ \beta \end{pmatrix} * \begin{pmatrix} \gamma \\ \delta \end{pmatrix} &= \begin{pmatrix} 1+\gamma\delta & -\gamma^2 \\ \delta^2 & 1-\gamma\delta \end{pmatrix} \begin{pmatrix} \alpha \\ \beta \end{pmatrix} \in (\mathbb{C}^2\backslash\{0\})/\pm \\ &\longleftrightarrow \begin{pmatrix} 1+\gamma\delta & -\gamma^2 \\ \delta^2 & 1-\gamma\delta \end{pmatrix} \begin{pmatrix} 1+\alpha\beta & -\alpha^2 \\ \beta^2 & 1-\alpha\beta \end{pmatrix} \begin{pmatrix} 1+\gamma\delta & -\gamma^2 \\ \delta^2 & 1-\gamma\delta \end{pmatrix}^{-1} \\ &= \begin{pmatrix} \gamma \\ \delta \end{pmatrix} \begin{pmatrix} \alpha \\ \beta \end{pmatrix} \begin{pmatrix} \gamma \\ \delta \end{pmatrix}^{-1} \in \mathrm{PSL}(2,\mathbb{C}). \end{aligned}$$

The inverse operation is given by

$$\begin{pmatrix} \alpha \\ \beta \end{pmatrix} *^{-1} \begin{pmatrix} \gamma \\ \delta \end{pmatrix} = \begin{pmatrix} 1-\gamma\delta & \gamma^2 \\ -\delta^2 & 1+\gamma\delta \end{pmatrix} \begin{pmatrix} \alpha \\ \beta \end{pmatrix}.$$

From now on, we use the notation $\mathcal{P}$ instead of $(\mathbb{C}^2\backslash\{0\})/\pm$.

2.2 Link group and shadow-coloring

Consider a representation $\rho : \pi_1(L) \to \mathrm{PSL}(2,\mathbb{C})$ of a hyperbolic link L. We call ρ *boundary-parabolic* when the peripheral subgroup $\pi_1(\partial(\mathbb{S}^3\backslash L))$ of $\pi_1(L)$ maps to a subgroup of $\mathrm{PSL}(2,\mathbb{C})$ whose elements are all parabolic.

For a fixed oriented link diagram[2] D of L, Wirtinger presentation gives an algorithmic expression of $\pi_1(L)$. For each arc α_k of D, we draw a small arrow labelled a_k as in Figure 1, which presents a loop. (The details are in [13]. Here we are using the opposite orientation of a_k to be consistent with the operation of the conjugation quandle.) This loop corresponds to one of the meridian curves of the boundary tori, so $\rho(a_k)$ is an element in $\mathcal{P}$. Hence we call $\{\rho(a_1), \ldots, \rho(a_n)\}$ *arc-coloring*[3] of D, whereas each $\rho(a_k)$ is assigned to the corresponding arc α_k.

Wirtinger presentation of the link group is given by

$$\pi_1(L) =< a_1, \ldots, a_n; r_1, \ldots, r_n >,$$

where the relation r_l is assigned to each crossing as in Figure 2. Note that r_l coincides with (2), so we can write down relation of the arc-colors as in Figure 3.

[2] We always assume the diagram does not contain a trivial knot component which has only over-crossings or under-crossings or no crossing. (For example, any unseparable link diagram satisfies this condition.) If it happens, then we change the diagram of the trivial component slightly. For example, applying Reidemeister second move to make different types of crossings or Reidemeister first move to add a kink is good enough. This assumption is necessary to guarantee that the octahedral triangulation becomes a topological triangulation of $\mathbb{S}^3\backslash(L \cup \{\text{two points}\})$

[3] Strictly speaking, arc-coloring is a map from arcs of D to $\mathcal{P}$, not a set. (Region-coloring, which will be defined below, is also a map from regions of D to $\mathcal{P}$.) However, we abuse the set notation here for convenience.

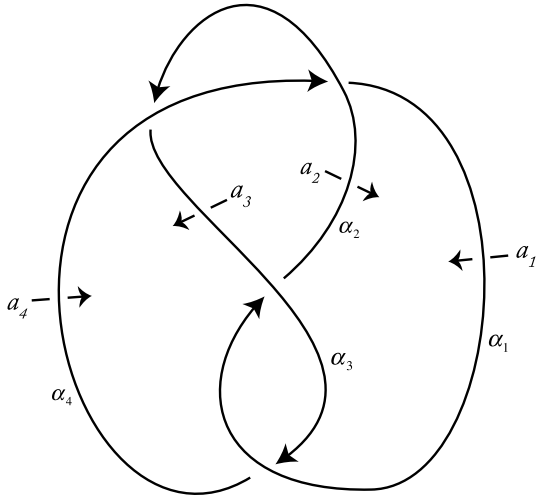

Figure 1: The figure-eight knot 4_1

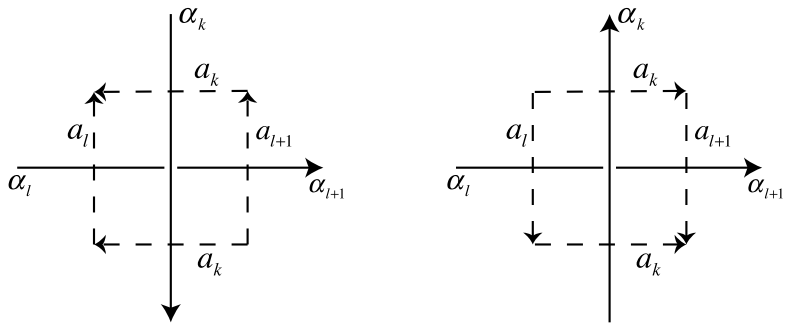

(a) $r_l : a_{l+1} = a_k a_l a_k^{-1}$ (b) $r_l : a_l = a_k a_{l+1} a_k^{-1}$

Figure 2: Relations at crossings

From now on, we always assume $\rho : \pi_1(L) \to \mathrm{PSL}(2, \mathbb{C})$ is a given boundary-parabolic representation. To avoid redundant notations, arc-color is denoted by $\{a_1, \ldots, a_n\}$ without ρ from now on. Choose an element $s \in \mathcal{P}$ corresponding to certain region of the diagram D and determine elements corresponding to the other regions using the relation in Figure 4.

The assignment of elements of $\mathcal{P}$ to all regions using the relation in Figure 4 is called *the region-coloring*. This assignment is well-defined because the two curves in Figure 5, which we call *the cross-changing pair*, determine the same region-coloring, and any pair of curves with the same starting and ending points can be transformed each other by finite sequence of cross-changing pairs.

An arc-coloring together with a region-coloring is called *shadow-coloring*. The following lemma shows important property of shadow-colorings, which is crucial for showing the existence of solutions of certain equations.

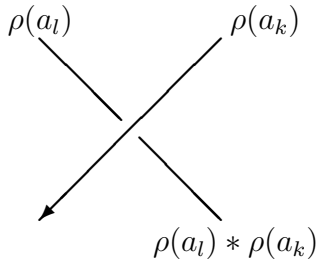

Figure 3: Arc-coloring

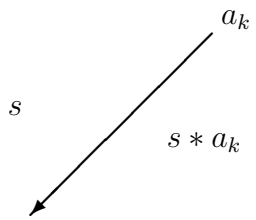

Figure 4: Region-coloring

Definition 2.3. *The* ***Hopf map*** $h : \mathcal{P} \longrightarrow \mathbb{CP}^1 = \mathbb{C} \cup \{\infty\}$ *is defined by*

$$\begin{pmatrix} \alpha \\ \beta \end{pmatrix} \mapsto \frac{\alpha}{\beta}.$$

Lemma 2.4. *Let L be a link and assume an arc-coloring is already given by the boundary-parabolic representation $\rho : \pi_1(L) \longrightarrow \mathrm{PSL}(2, \mathbb{C})$. Then, for any triple $(a_k, s, s * a_k)$ of an arc-color a_k and its surrounding region-colors $s, s * a_k$ as in Figure 4, there exists a region-coloring satisfying*

$$h(a_k) \neq h(s) \neq h(s * a_k) \neq h(a_k). \tag{4}$$

Proof. Note that this was already proved inside the proof of Proposition 2 of [9]. However, singling out the proof is not easy, so we write it down below for the readers' convenience.

For the given arc-colors $a_1, \ldots, a_n$, we choose region-colors $s_1, \ldots, s_m$ so that

$$\{h(s_1), \ldots, h(s_m)\} \cap \{h(a_1), \ldots, h(a_n)\} = \emptyset. \tag{5}$$

This is always possible because, the number of $h(s_1)$ satisfying $h(s_1) \in \{h(a_1), \ldots, h(a_n)\}$ is finite, and $h(s_2), \ldots, h(s_m)$ are uniquely determined by $h(s_1)$. Therefore, the number of $h(s_1)$ satisfying

$$\{h(s_1), \ldots, h(s_m)\} \cap \{h(a_1), \ldots, h(a_n)\} \neq \emptyset$$

is finite, but we have infinite freedom to choose $h(s_1) \in \mathbb{CP}^1$.

Now consider the case of Figure 4 and assume $h(s * a_k) = h(s)$. Then we obtain

$$h(s * a_k) = \widehat{a_k}(h(s)) = h(s), \tag{6}$$

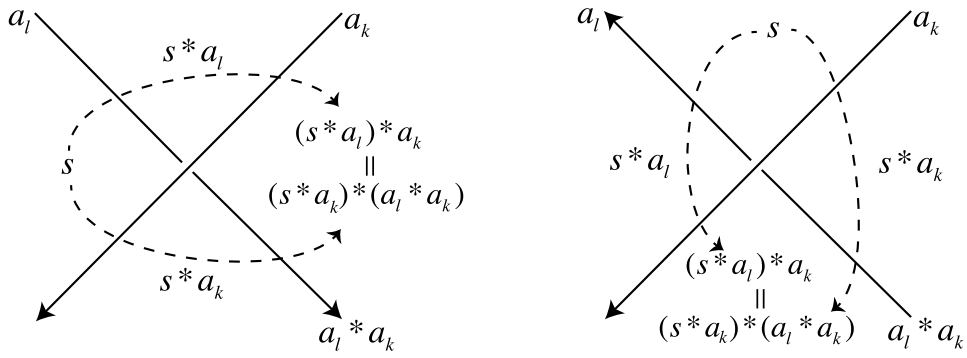

(a) Positive crossing (b) Negative crossing

Figure 5: Well-definedness of region-coloring

where $\widehat{a_k} : \mathbb{CP}^1 \to \mathbb{CP}^1$ is the Möbius transformation

$$\widehat{a_k}(z) = \frac{(1 + \alpha_k\beta_k)z - \alpha_k^2}{\beta_k^2 z + (1 - \alpha_k\beta_k)}$$

of $a_k = \begin{pmatrix} \alpha_k \\ \beta_k \end{pmatrix}$. Then (6) implies $h(s)$ is the fixed point of $\widehat{a_k}$, which means $h(a_k) = h(s)$ that contradicts (5).

□

We remark that the condition (5) is stronger than what we actually need in (4). Even though some region-coloring does not satisfy (5), if it satisfies (4), then all results of this article are applicable. Examples in Section 4 are of this type.

The arc-coloring induced by ρ together with the region-coloring satisfying Lemma 2.4 is called the *shadow-coloring induced by* ρ. This shadow-coloring will determine the exact coordinates of points of the octahedral triangulation in the next section.

2.3 Octahedral triangulations of link complements

In this section, we describe the ideal triangulation of $\mathbb{S}^3 \backslash (L \cup \{\text{two points}\})$ appeared in [4].

To obtain the triangulation, we consider the crossing j in Figure 6 and place an octahedron $\mathrm{A}_j\mathrm{B}_j\mathrm{C}_j\mathrm{D}_j\mathrm{E}_j\mathrm{F}_j$ on each crossing j as in Figure 7(a). Then we twist the octahedron by identifying edges $\mathrm{B}_j\mathrm{F}_j$ to $\mathrm{D}_j\mathrm{F}_j$ and $\mathrm{A}_j\mathrm{E}_j$ to $\mathrm{C}_j\mathrm{E}_j$, respectively. The edges $\mathrm{A}_j\mathrm{B}_j$, $\mathrm{B}_j\mathrm{C}_j$, $\mathrm{C}_j\mathrm{D}_j$ and $\mathrm{D}_j\mathrm{A}_j$ are called *horizontal edges* and we sometimes express these edges in the diagram as arcs around the crossing as in Figure 6.

Then we glue faces of the octahedra following the lines of the link diagram. Specifically, there are three gluing patterns as in Figure 8. In each cases (a), (b) and (c), we identify the faces $\triangle\mathrm{A}_j\mathrm{B}_j\mathrm{E}_j \cup \triangle\mathrm{C}_j\mathrm{B}_j\mathrm{E}_j$ to $\triangle\mathrm{C}_{j+1}\mathrm{D}_{j+1}\mathrm{F}_{j+1} \cup \triangle\mathrm{C}_{j+1}\mathrm{B}_{j+1}\mathrm{F}_{j+1}$, $\triangle\mathrm{B}_j\mathrm{C}_j\mathrm{F}_j \cup \triangle\mathrm{D}_j\mathrm{C}_j\mathrm{F}_j$ to $\triangle\mathrm{D}_{j+1}\mathrm{C}_{j+1}\mathrm{F}_{j+1} \cup \triangle\mathrm{B}_{j+1}\mathrm{C}_{j+1}\mathrm{F}_{j+1}$ and $\triangle\mathrm{A}_j\mathrm{B}_j\mathrm{E}_j \cup \triangle\mathrm{C}_j\mathrm{B}_j\mathrm{E}_j$ to $\triangle\mathrm{C}_{j+1}\mathrm{B}_{j+1}\mathrm{E}_{j+1} \cup \triangle\mathrm{A}_{j+1}\mathrm{B}_{j+1}\mathrm{E}_{j+1}$, respectively.

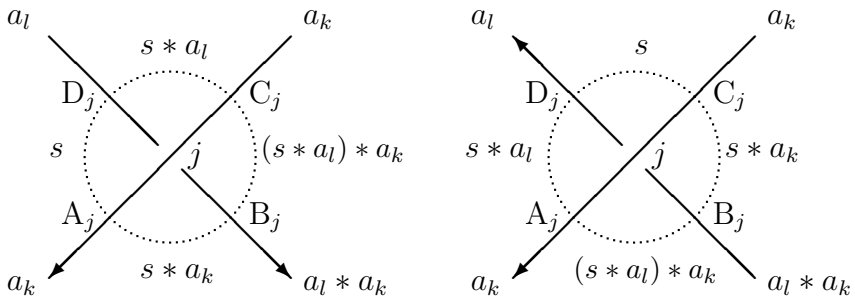

(a) Positive crossing (b) Negative crossing

Figure 6: Crossing j with shadow-coloring

Note that this gluing process identifies vertices $\{\mathrm{A}_j, \mathrm{C}_j\}$ to one point, denoted by $-\infty$, and $\{\mathrm{B}_j, \mathrm{D}_j\}$ to another point, denoted by ∞, and finally $\{\mathrm{E}_j, \mathrm{F}_j\}$ to the other points, denoted by P_t where $t = 1, \ldots, c$ and c is the number of the components of the link L. The regular neighborhoods of $-\infty$ and ∞ are two 3-balls and that of $\cup_{t=1}^{c} P_t$ is a tubular neighborhood of the link L. Therefore, after removing all vertices of the gluing, we obtain an *octahedral decomposition* of $\mathbb{S}^3 \backslash (L \cup \{\pm\infty\})$. The *octahedral triangulation* is obtained by subdividing each octahedron of the decomposition into four tetrahedra in certain way. To specify the subdivision, we consider a boundary-parabolic representation ρ is given and one shadow-coloring induced by ρ is fixed.

If $h(a_k) \neq h(a_l)$ in Figure 6, then we subdivide the octahedron into four tetrahedra by adding edge $\mathrm{E}_j\mathrm{F}_j$ as in Figure 7(b). Also, if $h(a_k) = h(a_l)$, then we subdivide it by adding edge $\mathrm{A}_j\mathrm{C}_j$ as in Figure 7(c). The result is called *the octahedral triangulation* of $\mathbb{S}^3 \backslash (L \cup \{\pm\infty\})$.

Consider the shadow-coloring of a link diagram D induced by ρ, and let $\{a_1, a_2, \ldots, a_n\}$ be the arc-colors and $\{s_1, s_2, \ldots, s_m\}$ be the region-colors. The number of these colors is finite, so can choose an element $p \in \mathcal{P}$ satisfying

$$h(p) \notin \{h(a_1), \ldots, h(a_n), h(s_1), \ldots, h(s_m)\}. \tag{7}$$

The geometric shape of the triangulation is determined by the shadow-coloring induced by ρ in the following way. If $h(a_k) \neq h(a_l)$ and the crossing j is positive, then let the signed coordinates of the tetrahedra $\mathrm{E}_j\mathrm{F}_j\mathrm{C}_j\mathrm{D}_j$, $\mathrm{E}_j\mathrm{F}_j\mathrm{A}_j\mathrm{D}_j$, $\mathrm{E}_j\mathrm{F}_j\mathrm{A}_j\mathrm{B}_j$, $\mathrm{E}_j\mathrm{F}_j\mathrm{C}_j\mathrm{B}_j$ be

$$(a_l, a_k, s * a_l, p), -(a_l, a_k, s, p), (a_l * a_k, a_k, s * a_k, p), -(a_l * a_k, a_k, (s * a_l) * a_k, p), \tag{8}$$

respectively. Here, the minus sign of the coordinate means the orientation of the tetrahedron does not coincide with the one induced by the vertex-ordering. Also, if the crossing j is negative, then let the signed coordinates of the tetrahedra $\mathrm{E}_j\mathrm{F}_j\mathrm{C}_j\mathrm{D}_j$, $\mathrm{E}_j\mathrm{F}_j\mathrm{A}_j\mathrm{D}_j$, $\mathrm{E}_j\mathrm{F}_j\mathrm{A}_j\mathrm{B}_j$, $\mathrm{E}_j\mathrm{F}_j\mathrm{C}_j\mathrm{B}_j$ be

$$(a_l, a_k, s, p), -(a_l, a_k, s * a_l, p), (a_l * a_k, a_k, (s * a_l) * a_k, p), -(a_l * a_k, a_k, s * a_k, p), \tag{9}$$

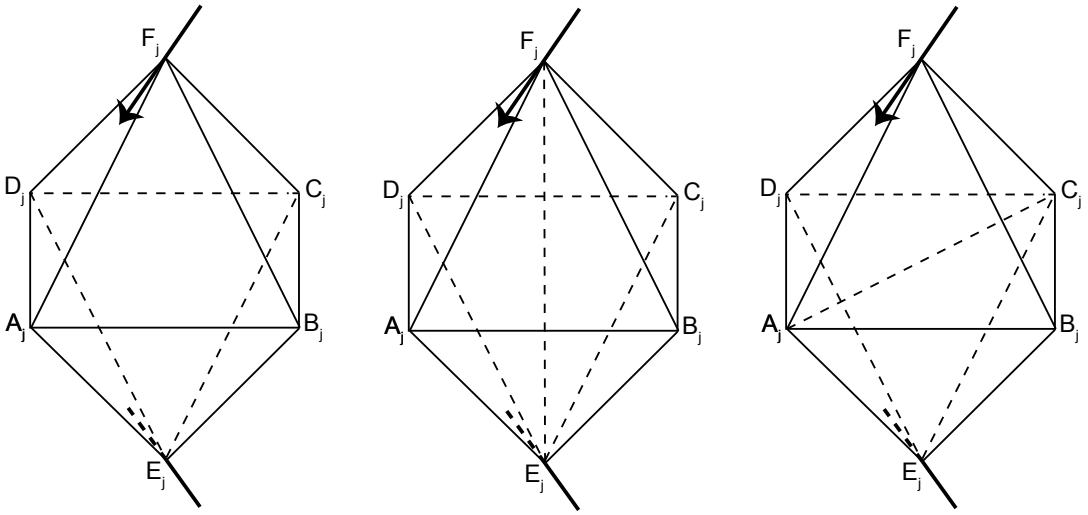

(a) (b) (c)

Figure 7: Octahedron on the crossing j

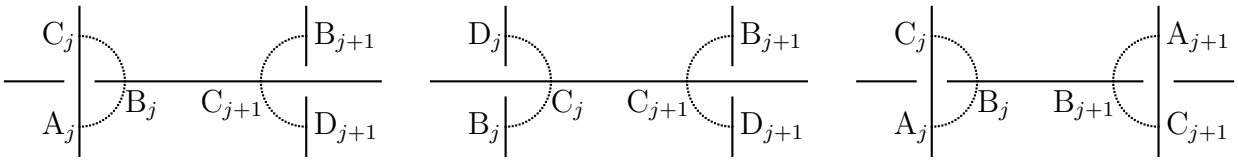

(a) (b) (c)

Figure 8: Three gluing patterns

respectively. Figures 9–10 show the signed coordinates of (8) and (9).

On the other hand, if $h(a_k) = h(a_l)$ and j is positive, then let the signed coordinates of the tetrahedra $\mathrm{F}_j\mathrm{A}_j\mathrm{C}_j\mathrm{D}_j$, $\mathrm{E}_j\mathrm{A}_j\mathrm{C}_j\mathrm{D}_j$, $\mathrm{E}_j\mathrm{A}_j\mathrm{C}_j\mathrm{B}_j$, $\mathrm{F}_j\mathrm{A}_j\mathrm{C}_j\mathrm{B}_j$ be

$$-(a_k, s, s*a_l, p), (a_l, s, s*a_l, p), -(a_l*a_k, s*a_k, (s*a_l)*a_k, p), (a_k, s*a_k, (s*a_l)*a_k, p), \quad (10)$$

respectively. If j is negative, then let the signed coordinates be

$$-(a_k, s*a_l, s, p), (a_l, s*a_l, s, p), -(a_l*a_k, (s*a_l)*a_k, s*a_k, p), (a_k, (s*a_l)*a_k, s*a_k, p), \quad (11)$$

respectively.

Figure 11 shows the signed coordinates of (10) and (11). Note that the orientations of (8)–(11) are different from [9] and match with [4].

We remark that the signed coordinates (8)–(11) actually define an element in certain simplicial quandle homology at [9]. Although this homology is crucial for proving the main results of [9], we will just use their results without considering the homology.

Definition 2.5. *Let $v_0, v_1, v_2, v_3 \in \mathbb{CP}^1 = \mathbb{C} \cup \{\infty\} = \partial\mathbb{H}^3$. The hyperbolic ideal tetrahedron with signed coordinate $\sigma(v_0, v_1, v_2, v_3)$ with $\sigma \in \{\pm 1\}$ is called* ***degenerate*** *when some of the*

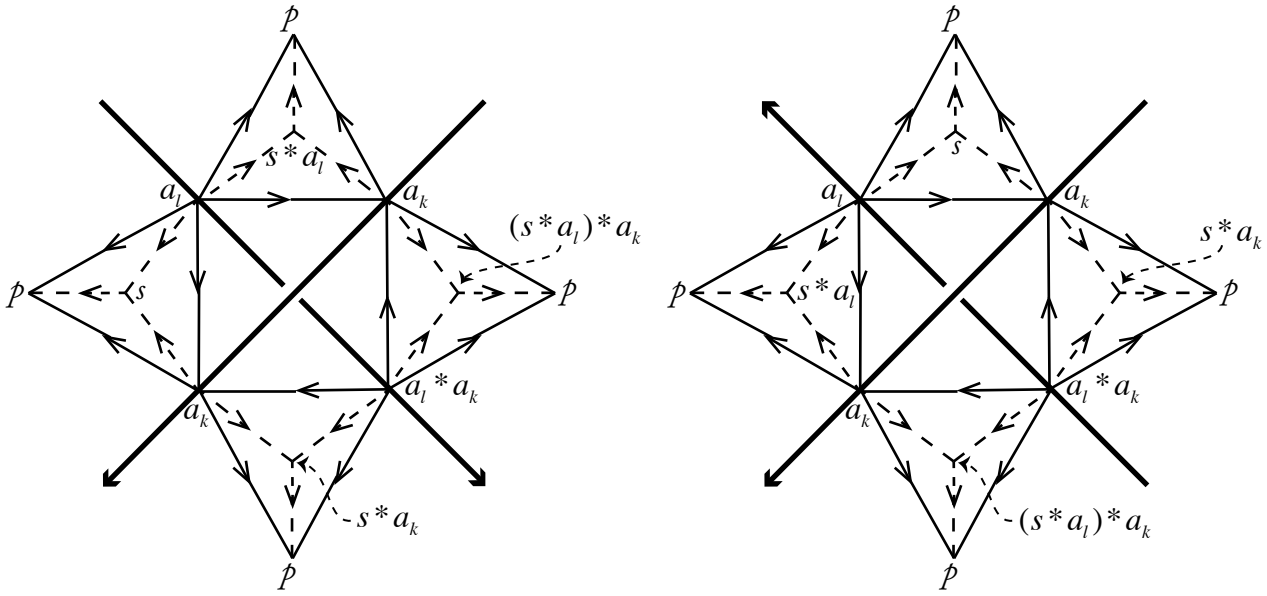

(a) Positive crossing (b) Negative crossing

Figure 9: Cooridnates of tetrahedra when $h(a_k) \neq h(a_l)$

vertices v_0, v_1, v_2, v_3 have the same coordinate, and ***non-degenerate*** *when all the vertices have different coordinates.* ***The cross-ratio*** *$[v_0, v_1, v_2, v_3]^\sigma$ of the non-degenerate signed coordinate $\sigma(v_0, v_1, v_2, v_3)$ is defined by*

$$[v_0, v_1, v_2, v_3]^\sigma = \left(\frac{v_3 - v_0}{v_2 - v_0} \frac{v_2 - v_1}{v_3 - v_1} \right)^\sigma \in \mathbb{C} \backslash \{0, 1\}.$$

The tetrahedra in (8)–(11) have elements of the coordinates in $\mathcal{P}$. Therefore, we need to send them to points in the boundary of the hyperbolic 3-space $\partial\mathbb{H}^3$ so as to obtain hyperbolic ideal tetrahedra. The Hopf map h, defined in Definition 2.3, plays the role.

Lemma 2.6. *The images of (8)–(11) under the Hopf map h are non-degenerate tetrahedra. Specifically, if $h(a_k) \neq h(a_l)$ and the crossing j is positive, then*

$$\begin{aligned} &(h(a_l), h(a_k), h(s * a_l), h(p)), -(h(a_l), h(a_k), h(s), h(p)), \\ &(h(a_l * a_k), h(a_k), h(s * a_k), h(p)), -(h(a_l * a_k), h(a_k), h((s * a_l) * a_k), h(p)), \end{aligned} \tag{12}$$

and, if $h(a_k) \neq h(a_l)$ and the crossing j is negative, then

$$\begin{aligned} &(h(a_l), h(a_k), h(s), h(p)), -(h(a_l), h(a_k), h(s * a_l), h(p)), \\ &(h(a_l * a_k), h(a_k), h((s * a_l) * a_k), h(p)), -(h(a_l * a_k), h(a_k), h(s * a_k), h(p)), \end{aligned} \tag{13}$$

are non-degenerate hyperbolic ideal tetrahedra.

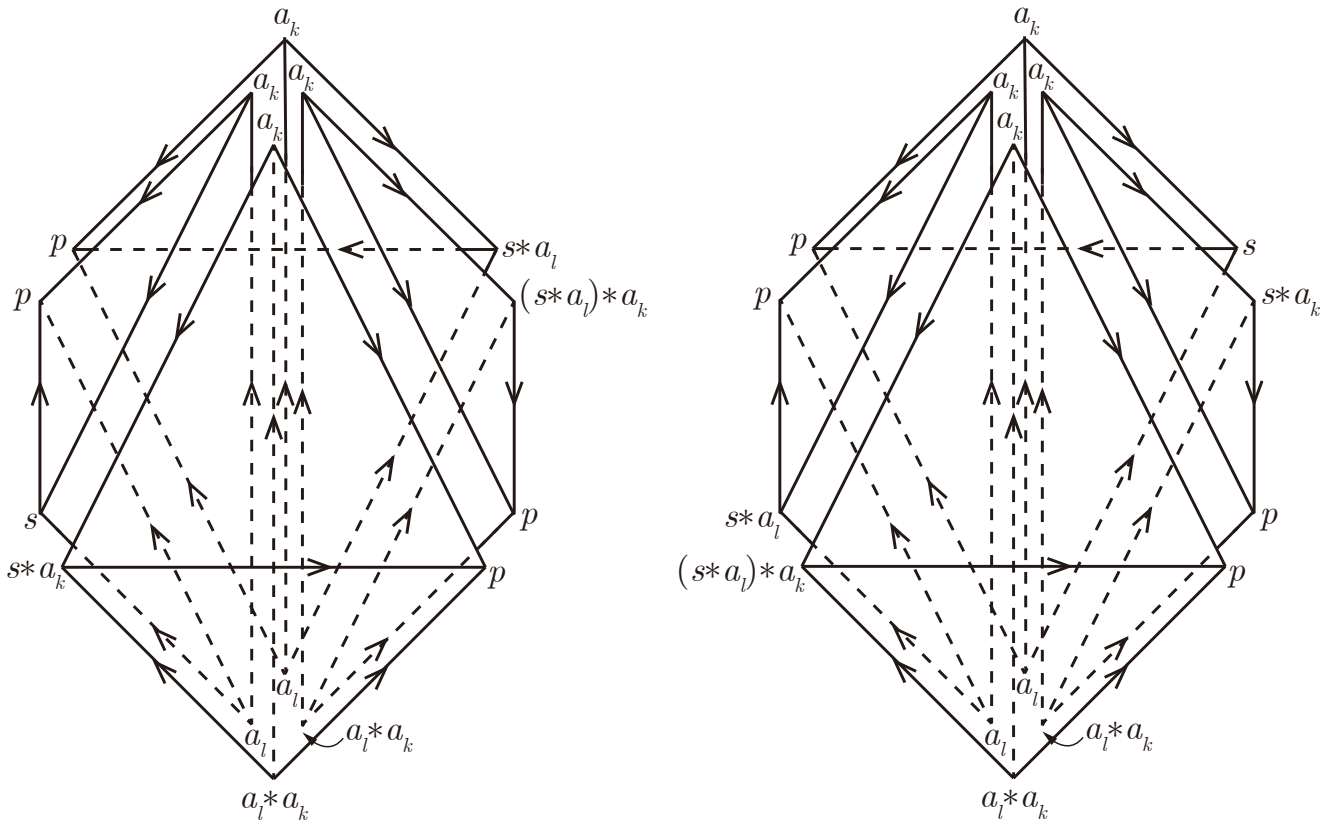

(a) Positive crossing

(b) Negative crossing

Figure 10: Figure 9 in octahedral position

If $h(a_k) = h(a_l)$ and the crossing j is positive, then

$$(h(a_l), h(s), h(s*a_l), h(p)), -(h(a_k), h(s), h(s*a_l), h(p)), \quad (14)$$
$$(h(a_k), h(s*a_k), h((s*a_l)*a_k), h(p)), -(h(a_l*a_k), h(s*a_k), h((s*a_l)*a_k), h(p)),$$

and, if $h(a_k) = h(a_l)$ and the crossing j is negative, then

$$(h(a_l), h(s*a_l), h(s), h(p)), -(h(a_k), h(s*a_l), h(s), h(p)), \quad (15)$$
$$(h(a_k), h((s*a_l)*a_k), h(s*a_k), h(p)), -(h(a_l*a_k), h((s*a_l)*a_k), h(s*a_k), h(p)),$$

are non-degenerate hyperbolic ideal tetrahedra.

Proof. Note that the shadow-coloring we are considering satisfies Lemma 2.4. To show the non-degeneracy, it is enough to show any two endpoints of an edge are different.

In the cases of (12)–(13), endpoints of any edge are adjacent, as a pair among $a_k, s, s*a_k$ in Figure 4 (to check the adjacency, refer Figure 5), or one of them is p, except the edges (a_l, a_k), $(a_l * a_k, a_k)$. Therefore, it is enough to show that $h(a_k) \neq h(a_l)$ implies $h(a_l * a_k) \neq h(a_k)$, which is trivial because $h(a_l * a_k) = h(a_k * a_k)$ implies $h(a_l) = h(a_k)$.

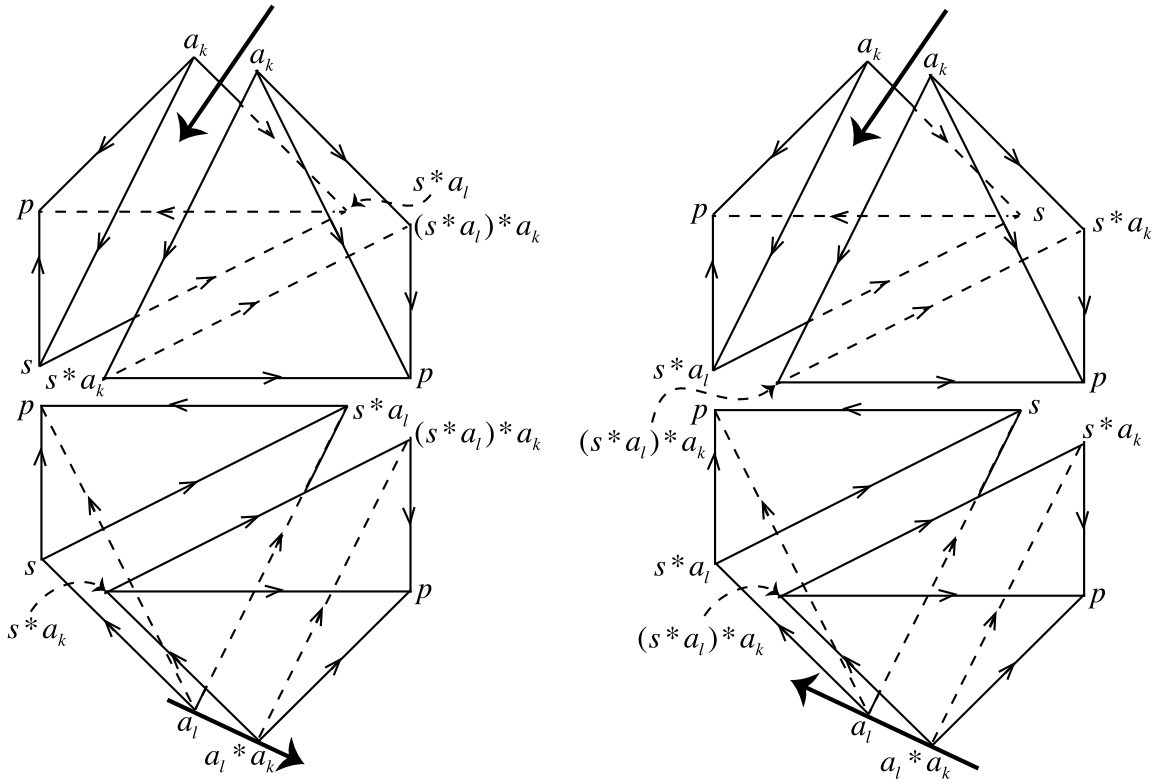

(a) Positive crossing (b) Negative crossing

Figure 11: Cooridnates of tetrahedra when $h(a_k) = h(a_l)$

In the cases of (14)–(15), all endpoints of edges are adjacent or one of them is p, so we get the proof.

□

Note that, when $h(a_k) = h(a_l)$, the first two tetrahedra in (14) share the same coordinate with different signs and the other two do the same. Therefore, all tetrahedra cancel each other out geometrically, so we can remove the octahedron of the crossing. Also, the same holds for (15). Removing these octahedra geometrically will be used crucially at many proofs in Section 3. (This idea induces many technical problems.)

When a geometric shape of a triangulation is given, it determines another representation $\rho' : \pi_1(L) \to \mathrm{PSL}(2, \mathbb{C})$ by the Yoshida's construction in Section 4.5 of [11]. However, ρ' should be conjugate with ρ because our construction of the geometric shape actually follows the construction of the developing map D_ρ introduced at Section 4.1 of [15].

2.4 Complex volume of ρ

Consider an ideal tetrahedron with vertices v_0, v_1, v_2, v_3, where $v_k \in \mathbb{CP}^1$. For each edge $v_k v_l$, we assign g_{kl} and $\widehat{g}_{kl} \in \mathbb{CP}^1$, and call them *long-edge parameter* and *edge parameter*,

respectively. (See Figure 12.) Later, we will distinguish them by considering g_{kl} is assigned to the edge of a triangulation and $\widehat{g}_{kl}$ to the edge of a tetrahedron.

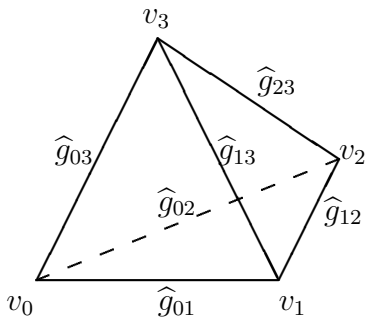

Figure 12: Edge parameter

Definition 2.7. *For the edge parameter $\widehat{g}_{kl}$ of an ideal tetrahedron,* ***Ptolemy identity*** *is the following equation:*

$$\widehat{g}_{02}\widehat{g}_{13} = \widehat{g}_{01}\widehat{g}_{23} + \widehat{g}_{03}\widehat{g}_{12}.$$

For example, if we define edge parameter $\widehat{g}_{kl} := v_l - v_k$, then direct calculation shows

$$(v_2 - v_0)(v_3 - v_1) = (v_1 - v_0)(v_3 - v_2) + (v_3 - v_0)(v_2 - v_1), \tag{16}$$

which is the Ptolemy identity. Furthermore, these edge parameters satisfy

$$[v_0, v_1, v_2, v_3] = \frac{\widehat{g}_{03}\widehat{g}_{12}}{\widehat{g}_{02}\widehat{g}_{13}}. \tag{17}$$

The Ptolemy identity[4] and (17) are the most important properties. However, the edge parameters is not good enough because it depends on the tetrahedron that the edge belongs To apply the results of [15] and [8], the variable assigned to the edge should depend only on the edge of the triangulation, not of the tetrahedron. In other words, if two edges are glued in the triangulation, the assigned variable of these edges should be the same. We call this condition *the coincidence property*. When the edge-parameter satisfies the coincidence property, we call it *the long-edge parameter* and denote it by g_{kl}. (We also need extra condition that the orientations of the two glued edges induced by the vertex-orientations of each tetrahedra should coincide. However, the vertex-orientation in (12)–(15) always satisfy it.) Unfortunately, $g_{kl} := v_l - v_k$ does not satisfy this condition, so we will redefine the edge-parameter and the long-edge parameter using [9] as follows.

At first, consider two elements $a = \begin{pmatrix} \alpha_1 \\ \alpha_2 \end{pmatrix}, b = \begin{pmatrix} \beta_1 \\ \beta_2 \end{pmatrix}$ in $\mathcal{P}$. We define *determinant* $\det(a, b)$ by

$$\det(a, b) := \pm \det \begin{pmatrix} \alpha_1 & \beta_1 \\ \alpha_2 & \beta_2 \end{pmatrix} = \pm(\alpha_1\beta_2 - \beta_1\alpha_2).$$

[4]Ptolemy identity is not used in this article, but it will be used extensively at another article.

Note that the determinant is defined up to sign due to the choice of the representative $a = \begin{pmatrix} \alpha_1 \\ \alpha_2 \end{pmatrix} = \begin{pmatrix} -\alpha_1 \\ -\alpha_2 \end{pmatrix} \in \mathcal{P}$. To remove this ambiguity, we fix representatives[5] of arc-colors in $\mathbb{C}^2\backslash\{0\}$ once and for all. Then we fix a representative of one region-color, which uniquely determines the representatives of all the other region-colors by the arc-coloring. (This is due to the fact that $s * (\pm a) = s * a$ for any $s, a \in \mathbb{C}^2\backslash\{0\}$.)

After fixing all the representatives of shadow-colors, we obtain a well-defined determinant

$$\det(a, b) = \det \begin{pmatrix} \alpha_1 & \beta_1 \\ \alpha_2 & \beta_2 \end{pmatrix} = \alpha_1\beta_2 - \beta_1\alpha_2. \tag{18}$$

Lemma 2.8. *For $a, b, c \in \mathbb{C}^2\backslash\{0\}$, the determinant satisfies*

$$\det(a * c, b * c) = \det(a, b).$$

Proof. Let $a = \begin{pmatrix} \alpha_1 \\ \alpha_2 \end{pmatrix}$, $b = \begin{pmatrix} \beta_1 \\ \beta_2 \end{pmatrix}$, $c = \begin{pmatrix} \gamma_1 \\ \gamma_2 \end{pmatrix}$, and $C = \begin{pmatrix} 1 + \gamma_1\gamma_2 & -\gamma_1^2 \\ \gamma_2^2 & 1 - \gamma_1\gamma_2 \end{pmatrix}$. Then

$$\det(a * c, b * c) = \det(C \begin{pmatrix} \alpha_1 \\ \alpha_2 \end{pmatrix}, C \begin{pmatrix} \beta_1 \\ \beta_2 \end{pmatrix}) = \det C \cdot \det(a, b) = \det(a, b).$$

□

Consider the shadow-coloring and the coordinates of tetrahedra in Figure 9 (or Figure 10) and Figure 11. We define the edge parameter $\widehat{g}_{kl}$ using those coordinates. Specifically, when the signed coordinate of the tetrahedron is $\sigma(a_0, a_1, a_2, a_3)$ with $\sigma \in \{\pm 1\}$ and $a_k \in \mathbb{C}^2\backslash\{0\}$, we define the edge parameter by

$$\widehat{g}_{kl} = \det(a_k, a_l). \tag{19}$$

For example, the edge parameters of the tetrahedron $\mp(a_l, a_k, s, p)$ in the left-hand or the right-hand side of Figure 9 (or Figure 10) are defined by

$$\begin{aligned} \widehat{g}_{01} = \det(a_l, a_k), \quad \widehat{g}_{02} = \det(a_l, s), \quad \widehat{g}_{03} = \det(a_l, p), \\ \widehat{g}_{12} = \det(a_k, s), \quad \widehat{g}_{13} = \det(a_k, p), \quad \widehat{g}_{23} = \det(s, p). \end{aligned}$$

Lemma 2.9. *The edge parameter $\widehat{g}_{kl}$ of the tetrahedron $\sigma(a_0, a_1, a_2, a_3)$ defined in (19) satisfies the Ptolemy identity and*

$$[h(a_0), h(a_1), h(a_2), h(a_3)] = \frac{\widehat{g}_{03}\widehat{g}_{12}}{\widehat{g}_{02}\widehat{g}_{13}}. \tag{20}$$

Proof. From (18), we obtain

$$h(x) - h(y) = \frac{x_1}{x_2} - \frac{y_1}{y_2} = \frac{\det(x, y)}{x_2 y_2}, \tag{21}$$

[5] The difference with [9] is that they chose a sign of the determinant once and for all. Their choice is good enough to define long-edge parameter g_{jk}, but not for edge parameter $\widehat{g}_{jk}$.

where $x = \begin{pmatrix} x_1 \\ x_2 \end{pmatrix}$ and $y = \begin{pmatrix} y_1 \\ y_2 \end{pmatrix}$.

Let $a_k = \begin{pmatrix} \alpha_k \\ \beta_k \end{pmatrix}$ for $k = 0, \dots, 3$, and let $v_k = h(a_k) = \frac{\alpha_k}{\beta_k}$. Then (16) and (21) imply

$$\frac{\det(a_0, a_2)}{\beta_0\beta_2}\frac{\det(a_1, a_3)}{\beta_1\beta_3} = \frac{\det(a_0, a_1)}{\beta_0\beta_1}\frac{\det(a_2, a_3)}{\beta_2\beta_3} + \frac{\det(a_0, a_3)}{\beta_0\beta_3}\frac{\det(a_1, a_2)}{\beta_1\beta_2},$$

which is equivalent to the Ptolemy identity $\widehat{g}_{02}\widehat{g}_{13} = \widehat{g}_{01}\widehat{g}_{23} + \widehat{g}_{03}\widehat{g}_{12}$.

Also, using (21), we obtain

$$[h(a_0), h(a_1), h(a_2), h(a_3)] = \frac{\frac{\det(a_0,a_3)}{\beta_0\beta_3}\frac{\det(a_1,a_2)}{\beta_1\beta_2}}{\frac{\det(a_1,a_3)}{\beta_1\beta_3}\frac{\det(a_0,a_2)}{\beta_0\beta_2}} = \frac{\widehat{g}_{03}\widehat{g}_{12}}{\widehat{g}_{02}\widehat{g}_{13}}.$$

□

Note that, by the same calculation of the proof above, we obtain

$$[h(a_0), h(a_3), h(a_1), h(a_2)] = \frac{\widehat{g}_{02}\widehat{g}_{13}}{\widehat{g}_{01}\widehat{g}_{23}},\ [h(a_0), h(a_2), h(a_3), h(a_1)] = -\frac{\widehat{g}_{01}\widehat{g}_{23}}{\widehat{g}_{03}\widehat{g}_{12}}.$$

If we put $z^\sigma = [h(a_0), h(a_1), h(a_2), h(a_3)]$, using Ptolemy identity, the above equations are expressed by

$$z^\sigma = \frac{\widehat{g}_{03}\widehat{g}_{12}}{\widehat{g}_{02}\widehat{g}_{13}},\ \frac{1}{1-z^\sigma} = \frac{\widehat{g}_{02}\widehat{g}_{13}}{\widehat{g}_{01}\widehat{g}_{23}},\ 1 - \frac{1}{z^\sigma} = -\frac{\widehat{g}_{01}\widehat{g}_{23}}{\widehat{g}_{03}\widehat{g}_{12}}. \tag{22}$$

The edge parameter $\widehat{g}_{jk}$ defined above satisfies all needed properties of the long-edge parameter g_{jk} except *the coincidence property*, which $\widehat{g}_{jk}$ satisfies up to sign. To see this phenomenon, consider the two edges of Figure 9(a) as in Figure 13, which are glued in the triangulation. Assume the chosen representative of a_m in Figure 13 satisfies $a_m = -a_l * a_k \in \mathbb{C}^2\backslash\{0\}$. (This actually happens often and quite important. For example, the minus signs of (47) and (48) in Section 4 show this situation. It will be discussed seriously at later article.) Then the edge parameters satisfy

$$\widehat{g}_{01} = \det(a_l, a_k) = \det(a_l * a_k, a_k) = -\det(a_m, a_k) = -\widehat{g}'_{01}.$$

To obtain the long-edge parameter g_{jk}, we assign certain signs to the edge parameters

$$g_{jk} = \pm\widehat{g}_{jk},$$

so that the consistency property holds. Due to Lemma 6 of [9], any choice of values of g_{jk} determines the same complex volume. Actually, in Section 3, we do not need the exact values of g_{jk}, but we use the existence of them.

The relations (22) of the edge parameters become

$$z^\sigma = \pm\frac{g_{03}g_{12}}{g_{02}g_{13}},\ \frac{1}{1-z^\sigma} = \pm\frac{g_{02}g_{13}}{g_{01}g_{23}},\ 1 - \frac{1}{z^\sigma} = \pm\frac{g_{01}g_{23}}{g_{03}g_{12}}. \tag{23}$$

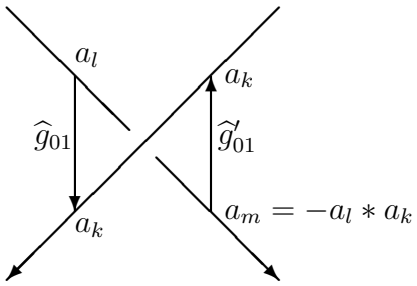

Figure 13: Example of the inconsistency of edge parameter

Using (23), we define integers p and q by

$$\begin{cases} p\pi i = -\log z^\sigma + \log g_{03} + \log g_{12} - \log g_{02} - \log g_{13}, \\ q\pi i = \log(1-z^\sigma) + \log g_{02} + \log g_{13} - \log g_{01} - \log g_{23}. \end{cases} \tag{24}$$

Now we consider the tetrahedron with the signed coordinate $\sigma(a_0, a_1, a_2, a_3)$ and the signed triples $\sigma[z^\sigma; p, q] \in \widehat{\mathcal{P}}(\mathbb{C})$. (*The extended pre-Bloch group* is denoted by $\widehat{\mathcal{P}}(\mathbb{C})$ here. For the definition, see Definition 1.6 of [15].) To consider all signed triples corresponding to all tetrahedra in the triangulation, we denote the triple by $\sigma_t[z_t^{\sigma_t}; p_t, q_t]$, where t is the index of tetrahedra. We define a function $\widehat{L} : \widehat{\mathcal{P}}(\mathbb{C}) \to \mathbb{C}/\pi^2\mathbb{Z}$ by

$$[z; p, q] \mapsto \mathrm{Li}_2(z) + \frac{1}{2}\log z \log(1-z) + \frac{\pi i}{2}(q \log z + p \log(1-z)) - \frac{\pi^2}{6}, \tag{25}$$

where $\mathrm{Li}_2(z) = -\int_0^z \frac{\log(1-t)}{t} dt$ is the dilogarithm function. (Well-definedness of $\widehat{L}$ was proved in [12].) Recall that, for a boundary-parabolic representation ρ, the hyperbolic volume $\mathrm{vol}(\rho)$ and the Chern-Simons invariant $\mathrm{cs}(\rho)$ was already defined in [15]. We call $\mathrm{vol}(\rho) + i\,\mathrm{cs}(\rho)$ *the complex volume of* ρ. The following theorem is one of the main result of [9].

Theorem 2.10 ([15], [9])**.** *For a given boundary-parabolic representation ρ and the shadow-coloring induced by ρ, the complex volume of ρ is calculated by*

$$\sum_t \sigma_t \widehat{L}[z_t^{\sigma_t}; p_t, q_t] \equiv i(\mathrm{vol}(\rho) + i\,\mathrm{cs}(\rho)) \pmod{\pi^2},$$

where t is over all tetrahedra of the triangulation defined in Section 2.3.

Proof. See Theorem 5 of [9].

□

Note that the removal of the tetrahedra in (14) and (15) does not have any effect on the complex volume. For example, if we put $[z; p, q]$ and $-[z'; p', q']$ the corresponding triples of the tetrahedron $(h(a_l), h(s), h(s * a_l), h(p))$ and $-(h(a_k), h(s), h(s * a_l), h(p))$ in (14), respectively, and put $\{g_{kl}\}, \{g'_{kl}\}$ the sets of long-edge parameters of the two tetrahedra, respectively. Then, from $h(a_l) = h(a_k)$, we obtain $z = z'$. Furthermore, we can choose long-edge parameters so that $g_{kl} = g'_{kl}$ holds for all pairs of edges sharing the same coordinate, which induces $p = p'$, $q = q'$ and $\widehat{L}[z; p, q] - \widehat{L}[z'; p', q'] = 0$.

3 Optimistic limit

In this Section, we will use the result of Section 2 to redefine the optimistic limit of [4] and construct a solution of $\mathcal{H}$. At first, we consider a given boundary-parabolic representation ρ and fix its shadow-coloring of a link diagram D. For the diagram, define sides of the diagram by the lines connecting two adjacent crossings. (The word *edge* is more common than *side* here. However, we want to keep the word *edge* for the edges of a triangulation.) For example, the diagram in Figure 14 has eight sides. We assign $z_1, \ldots, z_n$ to sides of D as in Figure 14 and call them *side variables*.

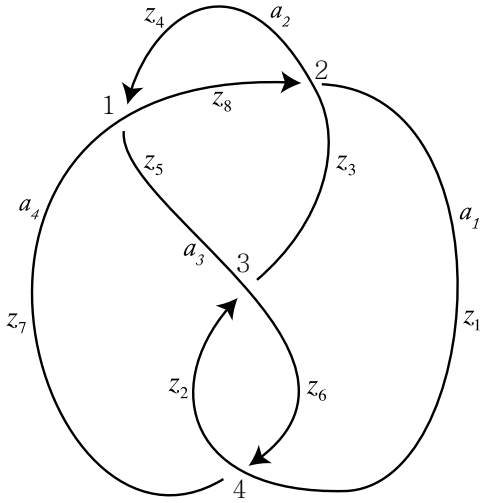

Figure 14: Sides of a link diagram

For the crossing j in Figure 15, let z_e, z_f, z_g, z_h be side variables and let a_l, a_k be the arc-colors. If $h(a_k) \neq h(a_l)$, then we define the potential function V_j of the crossing j by

$$V_j(z_e, z_f, z_g, z_h) = \mathrm{Li}_2(\frac{z_f}{z_e}) - \mathrm{Li}_2(\frac{z_f}{z_g}) + \mathrm{Li}_2(\frac{z_h}{z_g}) - \mathrm{Li}_2(\frac{z_h}{z_e}). \tag{26}$$

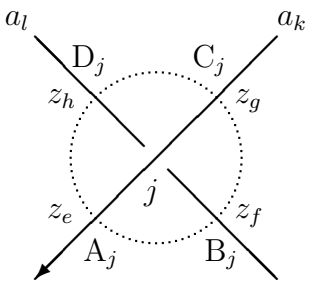

Figure 15: A crossing j with arc-colors and side variables

On the other hand, if $h(a_l) = h(a_k)$ in Figure 15, then we introduce new variables

w_e^j, w_f^j, w_g^j of the crossing j and define

$$\begin{aligned} &V_j(z_e, z_f, z_g, z_h, w_e^j, w_f^j, w_g^j) \\ &\quad = -\log w_e^j \log z_e + \log w_f^j \log z_f - \log w_g^j \log z_g + \log \frac{w_e^j w_g^j}{w_f^j} \log z_h. \end{aligned} \tag{27}$$

For notational convenience, we put $w_h^j := w_e^j w_g^j / w_f^j$. (In (27), we can choose any three variables among $w_e^j, w_f^j, w_g^j, w_h^j$ free variables.) We call the crossing j in Figure 15 *degenerate* when $h(a_l) = h(a_k)$ holds. In particular, when the degenerate crossing forms a kink, as in Figure 16, we put

$$\begin{aligned} &V_j(z_e, z_f, z_g, w_e^j, w_f^j) \\ &\quad = -\log w_e^j \log z_e + \log w_f^j \log z_f - \log w_f^j \log z_f + \log \frac{w_e^j w_f^j}{w_f^j} \log z_g \\ &\quad = -\log w_e^j \log z_e + \log w_e^j \log z_g. \end{aligned}$$

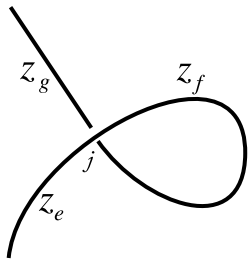

Figure 16: Kink

Consider the crossing j in Figure 15 and place the octahedron $\mathrm{A}_j\mathrm{B}_j\mathrm{C}_j\mathrm{D}_j\mathrm{E}_j\mathrm{F}_j$ as in Figure 7. When the crossing j is non-degenerate, in other words $h(a_k) \neq h(a_l)$, we consider Figure 7(b) and assign shape parameters $\frac{z_f}{z_e}$, $\frac{z_g}{z_f}$, $\frac{z_h}{z_g}$ and $\frac{z_e}{z_h}$ to the horizontal edges $\mathrm{A}_j\mathrm{B}_j$, $\mathrm{B}_j\mathrm{C}_j$, $\mathrm{C}_j\mathrm{D}_j$, $\mathrm{D}_j\mathrm{A}_j$, respectively. On the other hand, if the crossing j is degenerate, in other words $h(a_k) = h(a_l)$, then we consider Figure 7(c) and assign shape parameters w_e^j, w_f^j, w_g^j and w_h^j to the edges $\mathrm{A}_j\mathrm{F}_j$, $\mathrm{B}_j\mathrm{E}_j$, $\mathrm{C}_j\mathrm{F}_j$ and $\mathrm{D}_j\mathrm{E}_j$, respectively.[6]

The *potential function* $V(z_1, \ldots, z_n, w_k^j, \ldots)$ of the link diagram D is defined by

$$V(z_1, \ldots, z_n, w_k^j, \ldots) = \sum_j V_j,$$

[6] Note that, when $h(a_k) = h(a_l)$, by adding one more edge $\mathrm{B}_j\mathrm{D}_j$ to Figure 7(c), we obtain another subdivision of the octahedron with five tetrahedra. (This subdivision was already used in [1].) Focusing on the middle tetrahedron that contains all horizontal edges, we obtain $w_e^j w_g^j = w_f^j w_h^j$. Furthermore, the shape-parameters assigned to $\mathrm{D}_j\mathrm{F}_j$ and $\mathrm{B}_j\mathrm{F}_j$ are $\frac{1-1/w_e^j}{1-w_g^j}$ and $\frac{1-1/w_g^j}{1-w_e^j}$, respectively.

where j is over all crossings. For example, if $h(a_1) \neq h(a_2)$ in Figure 14, then $a_4 = a_1 * a_2$ implies[7] $h(a_4) \neq h(a_2)$, $a_2 = a_1 * a_3$ does[8] $h(a_2) \neq h(a_3) \neq h(a_1)$, $a_2 = a_3 * a_4$ does $h(a_4) \neq h(a_3)$, $a_4 = a_3 * a_1$ does $h(a_4) \neq h(a_1)$, and the potential function becomes

$$\begin{aligned} V(z_1, \ldots, z_8) &= \left\{ \mathrm{Li}_2(\frac{z_5}{z_7}) - \mathrm{Li}_2(\frac{z_5}{z_8}) + \mathrm{Li}_2(\frac{z_4}{z_8}) - \mathrm{Li}_2(\frac{z_4}{z_7}) \right\} \\ &+ \left\{ \mathrm{Li}_2(\frac{z_1}{z_3}) - \mathrm{Li}_2(\frac{z_1}{z_4}) + \mathrm{Li}_2(\frac{z_8}{z_4}) - \mathrm{Li}_2(\frac{z_8}{z_3}) \right\} \\ &+ \left\{ \mathrm{Li}_2(\frac{z_3}{z_6}) - \mathrm{Li}_2(\frac{z_3}{z_5}) + \mathrm{Li}_2(\frac{z_2}{z_5}) - \mathrm{Li}_2(\frac{z_2}{z_6}) \right\} \\ &+ \left\{ \mathrm{Li}_2(\frac{z_6}{z_1}) - \mathrm{Li}_2(\frac{z_6}{z_2}) + \mathrm{Li}_2(\frac{z_7}{z_2}) - \mathrm{Li}_2(\frac{z_7}{z_1}) \right\}. \end{aligned} \tag{28}$$

Note that, if $h(a_l) \neq h(a_k)$ for any crossing j in Figure 15, then the definition of the potential function above coincides with the definition in Section 2 of [4]. Therefore, the above definition is a slight modification of the previous one.

On the other hand, if $h(a_1) = h(a_2)$ in Figure 14, then $a_1 * a_2 = a_1$. This equation and the relations at crossings induce[9] $a_1 = a_2 = a_3 = a_4$, and the potential function becomes

$$\begin{aligned} &V(z_1, \ldots, z_8, w_8^1, w_4^1, w_7^1, w_4^2, w_8^2, w_3^2, w_6^3, w_3^3, w_5^3, w_2^4, w_7^4, w_1^4) \\ &\quad = -\log w_8^1 \log z_8 + \log w_4^1 \log z_4 - \log w_7^1 \log z_7 + \log w_5^1 \log z_5 \\ &\qquad - \log w_4^2 \log z_4 + \log w_8^2 \log z_8 - \log w_3^2 \log z_3 + \log w_1^2 \log z_1 \\ &\qquad - \log w_6^3 \log z_6 + \log w_3^3 \log z_3 - \log w_5^3 \log z_5 + \log w_2^3 \log z_2 \\ &\qquad - \log w_2^4 \log z_2 + \log w_7^4 \log z_7 - \log w_1^4 \log z_1 + \log w_6^4 \log z_6, \end{aligned}$$

where $w_5^1 = w_8^1 w_7^1 / w_4^1$, $w_1^2 = w_4^2 w_3^2 / w_8^2$, $w_2^3 = w_6^3 w_5^3 / w_3^3$ and $w_6^4 = w_2^4 w_1^4 / w_7^4$.

For the potential function $V(z_1, \ldots, z_n, w_k^j, \ldots)$, let $\mathcal{H}$ be the set of equations

$$\mathcal{H} := \left\{ \exp(z_k \frac{\partial V}{\partial z_k}) = 1, \exp(w_k^j \frac{\partial V}{\partial w_k^j}) = 1 \,\middle|\, k = 1, \ldots, n,\ j : \text{degenerate} \right\}, \tag{29}$$

and $\mathcal{S} = \{(z_1, \ldots, z_n, w_k^j, \ldots)\}$ be the solution set of $\mathcal{H}$. Here, solutions are assumed to satisfy the properties that $z_k \neq 0$ for all $k = 1, \ldots, n$ and $\frac{z_f}{z_e} \neq 1$, $\frac{z_g}{z_f} \neq 1$, $\frac{z_h}{z_g} \neq 1$, $\frac{z_e}{z_h} \neq 1$, $\frac{z_g}{z_e} \neq 1$, $\frac{z_h}{z_f} \neq 1$ in Figure 15 for any non-degenerate crossing, and $w_k^j \neq 0$ for any degenerate crossing j and the index k. (All these assumptions are essential to avoid singularity of the equations in $\mathcal{H}$ and $\log 0$ in the formula V_0 defined in (33). Even though we allow $w_k^j = 1$ here, the value we are interested in always satisfies $w_k^j \neq 1$.)

[7] If $h(a_4) = h(a_2)$, then $h(a_2 * a_2) = h(a_2) = h(a_4) = h(a_1 * a_2)$ induces $h(a_2) = h(a_1)$, which is contradiction.

[8] If $h(a_2) = h(a_3)$, then $h(a_3 * a_3) = h(a_3) = h(a_2) = h(a_1 * a_3)$ induces $h(a_2) = h(a_3) = h(a_1)$, which is contradiction. Likewise, if $h(a_1) = h(a_3)$, then $h(a_2) = h(a_1 * a_3) = h(a_1)$ is contradiction.

[9] The relation $a_4 = a_1 * a_2$ induces $a_4 = a_1$, $a_4 = a_3 * a_1$ does $a_4 = a_3$, and $a_2 = a_3 * a_4$ does $a_2 = a_4$.

Proposition 3.1. *For the arc-coloring of a link diagram D induced by ρ and the potential function $V(z_1, \ldots, z_n, w_k^j, \ldots)$, the set $\mathcal{H}$ induces the whole set of hyperbolicity equations of the octahedral triangulation defined in Section 2.3.*

The *hyperbolicity equations* consist of the Thurston's gluing equations of edges and the completeness condition.

Proof of Proposition 3.1. When no crossing is degenerate, this proposition was already proved in Section 3 of [4]. To see the main idea, check Figures 10–13 and equations (3.1)–(3.3) of [4]. Equation (3.1) is a completeness condition along a meridian of certain annulus, and (3.2)–(3.3) are gluing equations of certain edges. These three types of equations induce all the other gluing equations.

Therefore, we consider the case when the crossing j in Figure 15 is degenerate. Then, the following three equations

$$\exp(w_e^j \frac{\partial V}{\partial w_e^j}) = \frac{z_h}{z_e} = 1, \ \ \exp(w_f^j \frac{\partial V}{\partial w_f^j}) = \frac{z_f}{z_h} = 1, \ \ \exp(w_g^j \frac{\partial V}{\partial w_g^j}) = \frac{z_h}{z_g} = 1 \tag{30}$$

induce $z_e = z_f = z_g = z_h$. This guarantees the gluing equations of horizontal edges trivially by the assigning rule of shape parameters. (Note that the shape parameters assigned to the horizontal edges of the octahedron at a degenerate crossing are always 1.)

There are four possible cases of gluing pattern as in Figure 17, and we assume the crossing j is degenerate and $j+1$ is non-degenerate. (The case when both of j and $j+1$ are degenerate can be proved similarly.)

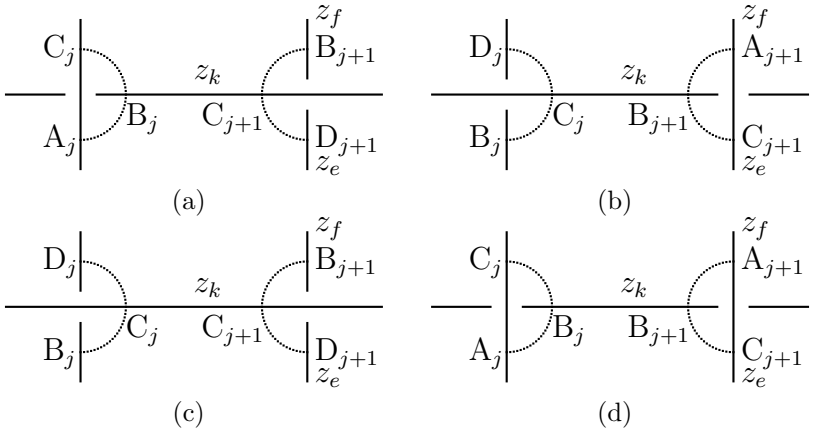

Figure 17: Four cases of gluing pattern

The part of the potential function V containing z_k in Figure 17(a) is

$$V^{(a)} = \log w_k^j \log z_k + \mathrm{Li}_2\left(\frac{z_e}{z_k}\right) - \mathrm{Li}_2\left(\frac{z_f}{z_k}\right),$$

and

$$\exp\left(z_k \frac{\partial V}{\partial z_k}\right) = \exp\left(z_k \frac{\partial V^{(a)}}{\partial z_k}\right) = w_k^j \left(1 - \frac{z_e}{z_k}\right)\left(1 - \frac{z_f}{z_k}\right)^{-1} = 1$$

is equivalent with the following completeness condition

$$\frac{1}{w_k^j}\left(1-\frac{z_e}{z_k}\right)^{-1}\left(1-\frac{z_f}{z_k}\right)=1$$

along a meridian m in Figure 18(a). (Compare it with Figure 11 of [4].) Here, a_j, b_j, c_j, b_{j+1}, c_{j+1}, d_{j+1} in Figure 18(a) are the points of the cusp diagram, which lie on the edges $\mathrm{A}_j\mathrm{E}_j$, $\mathrm{B}_j\mathrm{E}_j$, $\mathrm{C}_j\mathrm{E}_j$, $\mathrm{B}_{j+1}\mathrm{F}_{j+1}$, $\mathrm{C}_{j+1}\mathrm{F}_{j+1}$, $\mathrm{D}_{j+1}\mathrm{F}_{j+1}$ of Figure 7(a), respectively.

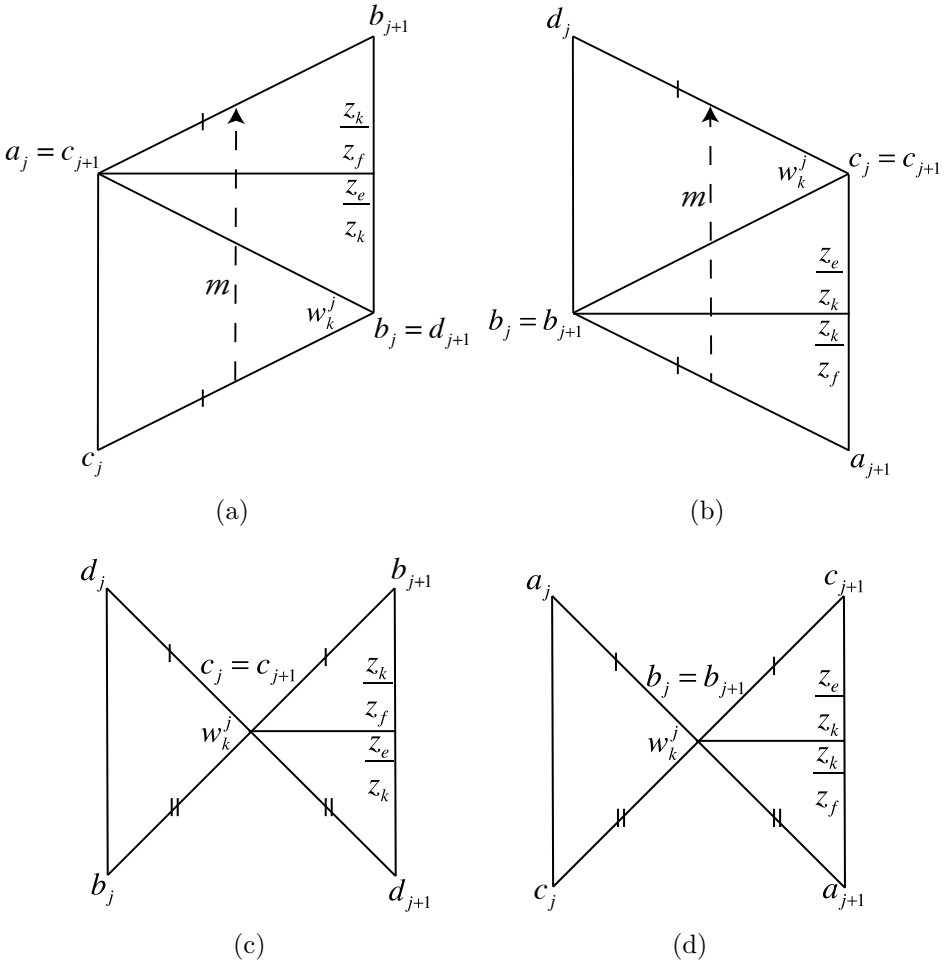

Figure 18: Four cusp diagrams from Figure 17

The part of the potential function V containing z_k in Figure 17(b) is

$$V^{(b)}=-\log w_k^j\log z_k-\mathrm{Li}_2\left(\frac{z_k}{z_e}\right)+\mathrm{Li}_2\left(\frac{z_k}{z_f}\right),$$

and

$$\exp\left(z_k\frac{\partial V}{\partial z_k}\right)=\exp\left(z_k\frac{\partial V^{(b)}}{\partial z_k}\right)=\frac{1}{w_k^j}\left(1-\frac{z_k}{z_e}\right)\left(1-\frac{z_k}{z_f}\right)^{-1}=1$$

is equivalent with the following completeness condition

$$\frac{1}{w_k^j}\left(1-\frac{z_k}{z_f}\right)^{-1}\left(1-\frac{z_k}{z_e}\right)=1$$

along a meridian m in Figure 18(b). Here, b_j, c_j, d_j, a_{j+1}, b_{j+1}, c_{j+1} in Figure 18(b) are the points of the cusp diagram, which lie on the edges $\mathrm{B}_j\mathrm{F}_j$, $\mathrm{C}_j\mathrm{F}_j$, $\mathrm{D}_j\mathrm{F}_j$, $\mathrm{A}_{j+1}\mathrm{E}_{j+1}$, $\mathrm{B}_{j+1}\mathrm{E}_{j+1}$, $\mathrm{C}_{j+1}\mathrm{E}_{j+1}$ of Figure 7(a), respectively. (To simplify the cusp diagram in Figure 18(b), we subdivided the polygon $\mathrm{A}_j\mathrm{B}_j\mathrm{C}_j\mathrm{D}_j\mathrm{F}_j$ in Figure 7(c) into three tetrahedra by adding the edge $\mathrm{B}_j\mathrm{D}_j$.)

The part of the potential function V containing z_k in Figure 17(c) is

$$V^{(c)}=-\log w_k^j\log z_k+\mathrm{Li}_2\left(\frac{z_e}{z_k}\right)-\mathrm{Li}_2\left(\frac{z_f}{z_k}\right),$$

and

$$\exp\left(z_k\frac{\partial V}{\partial z_k}\right)=\exp\left(z_k\frac{\partial V^{(c)}}{\partial z_k}\right)=\frac{1}{w_k^j}\left(1-\frac{z_e}{z_k}\right)\left(1-\frac{z_f}{z_k}\right)^{-1}=1$$

is equivalent with the following gluing equation

$$w_k^j\left(1-\frac{z_e}{z_k}\right)^{-1}\left(1-\frac{z_f}{z_k}\right)=1$$

of $c_j=c_{j+1}$ in Figure 18(c). (Compare it with Figure 12 of [4].) Here, b_j, c_j, d_j, b_{j+1}, c_{j+1}, d_{j+1} in Figure 18(c) are the points of the cusp diagram, which lie on the edges $\mathrm{B}_j\mathrm{F}_j$, $\mathrm{C}_j\mathrm{F}_j$, $\mathrm{D}_j\mathrm{F}_j$, $\mathrm{B}_{j+1}\mathrm{F}_{j+1}$, $\mathrm{C}_{j+1}\mathrm{F}_{j+1}$, $\mathrm{D}_{j+1}\mathrm{F}_{j+1}$ of Figure 7(a), respectively, and the edges d_jc_j and b_jc_j are identified to $b_{j+1}c_{j+1}$ and $d_{j+1}c_{j+1}$, respectively. (To simplify the cusp diagram in Figure 18(c), we subdivided the polygon $\mathrm{A}_j\mathrm{B}_j\mathrm{C}_j\mathrm{D}_j\mathrm{F}_j$ in Figure 7(c) into three tetrahedra by adding the edge $\mathrm{B}_j\mathrm{D}_j$.)

The part of the potential function V containing z_k in Figure 17(d) is

$$V^{(d)}=\log w_k^j\log z_k-\mathrm{Li}_2\left(\frac{z_k}{z_e}\right)+\mathrm{Li}_2\left(\frac{z_k}{z_f}\right),$$

and

$$\exp\left(z_k\frac{\partial V}{\partial z_k}\right)=\exp\left(z_k\frac{\partial V^{(d)}}{\partial z_k}\right)=w_k^j\left(1-\frac{z_k}{z_e}\right)\left(1-\frac{z_k}{z_f}\right)^{-1}=1$$

is equivalent with the following gluing equation

$$w_k^j\left(1-\frac{z_k}{z_e}\right)\left(1-\frac{z_k}{z_f}\right)^{-1}=1$$

of $b_j=b_{j+1}$ in Figure 18(d). (Compare it with Figure 13 of [4].) Here, a_j, b_j, c_j, a_{j+1}, b_{j+1}, c_{j+1} in Figure 18(d) are the points of the cusp diagram, which lie on the edges $\mathrm{A}_j\mathrm{E}_j$, $\mathrm{B}_j\mathrm{E}_j$,

C_jE_j, $A_{j+1}E_{j+1}$, $B_{j+1}E_{j+1}$, $C_{j+1}E_{j+1}$ of Figure 7(a), respectively, and the edges a_jb_j and c_jb_j are identified to $c_{j+1}b_{j+1}$ and $a_{j+1}b_{j+1}$, respectively.

Note that the case when both of the crossings j and $j+1$ in Figure 17 are degenerate can be proved by the same way.

On the other hand, it was already shown in [4] that all hyperbolicity equations are induced by these types of equations (see the discussion that follows Lemma 3.1 of [4]), so the proof is done.

□

In [4], we could not prove the existence of a solution of $\mathcal{H}$, in other words $\mathcal{S} \neq \emptyset$, so we assumed it. However, the following theorem proves the existence by directly constructing one solution from the given boundary-parabolic representation ρ together with the shadow-coloring.

Theorem 3.2. *Consider a shadow-coloring of a link diagram D induced by ρ which satisfies Lemma 2.4 and the potential function $V(z_1, \ldots, z_n, w_k^j, \ldots)$ from D. For each side of D with the side variable z_k, arc-color a_l and the region-color s, as in Figure 19, we define*

$$z_k^{(0)} := \frac{\det(a_l, p)}{\det(a_l, s)}. \tag{31}$$

Also, if the positive crossing j in Figure 20(a) is degenerate, then we define

$$(w_e^j)^{(0)} := \frac{\det(s, p)}{\det(s * a_k, p)},\ (w_f^j)^{(0)} := \frac{\det((s * a_l) * a_k, p)}{\det(s * a_k, p)},$$
$$(w_g^j)^{(0)} := \frac{\det((s * a_l) * a_k, p)}{\det(s * a_l, p)},\ (w_h^j)^{(0)} := \frac{\det(s, p)}{\det(s * a_l, p)},$$

and, if the negative crossing j in Figure 20(b) is degenerate, then we define

$$(w_e^j)^{(0)} := \frac{\det(s * a_l, p)}{\det((s * a_l) * a_k, p)},\ (w_f^j)^{(0)} := \frac{\det(s * a_k, p)}{\det((s * a_l) * a_k, p)},$$
$$(w_g^j)^{(0)} := \frac{\det(s * a_k, p)}{\det(s, p)},\ (w_h^j)^{(0)} := \frac{\det(s * a_l, p)}{\det(s, p)}.$$

Then $z_k^{(0)} \neq 0, 1, \infty$, $(w_k^j)^{(0)} \neq 0, 1$ for all possible j, k, and $(z_1^{(0)}, \ldots, z_n^{(0)}, (w_k^j)^{(0)}, \ldots) \in \mathcal{S}$.

Note that the $\pm$ signs in the arc-colors of Figure 20 appears due to the representatives of the colors in $\mathbb{C}^2\backslash\{0\}$. However, $\pm$ does not change the value of $z_k^{(0)}$ because

$$\frac{\det(\pm a_l, p)}{\det(\pm a_l, s)} = \frac{\det(a_l, p)}{\det(a_l, s)} = z_k^{(0)}.$$

Likewise, the value of $(w_k^j)^{(0)}$ does not depend on the choice of $\pm$ because the representatives of region-colors are uniquely determined from the fact $s * (\pm a) = s * a$ for any $s, a \in \mathbb{C}^2\backslash\{0\}$.

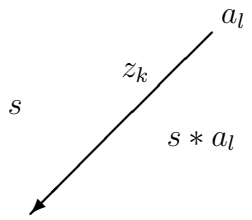

Figure 19: Region-coloring

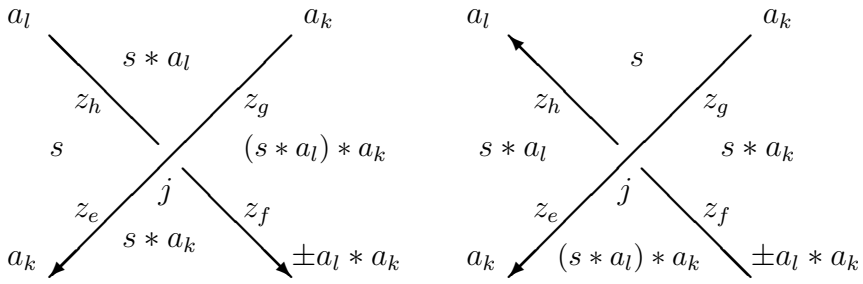

(a) Positive crossing (b) Negative crossing

Figure 20: Crossings with shadow-colors and side-variables

Proof of Theorem 3.2. At first, when the crossing j in Figure 20 is degenerate, we will show

$$z_e^{(0)} = z_f^{(0)} = z_g^{(0)} = z_h^{(0)}, \tag{32}$$

which satisfies (30). Using $h(a_k) = h(a_l)$, we put $a_k = \begin{pmatrix} \alpha \\ \beta \end{pmatrix}$ and $a_l = \begin{pmatrix} c\,\alpha \\ c\,\beta \end{pmatrix} = c\,a_k$ for some constant $c \in \mathbb{C}\backslash\{0\}$. Then we obtain $a_l * a_k = a_l$ and, if j is positive crossing, then

$$\begin{aligned}
z_e^{(0)} &= \frac{c\,\det(a_k, p)}{c\,\det(a_k, s)} = \frac{\det(a_l, p)}{\det(a_l, s)} = z_h^{(0)}, \\
z_f^{(0)} &= \frac{\det(\pm a_l * a_k, p)}{\det(\pm a_l * a_k, s * a_k)} = \frac{\det(a_l * a_k, p)}{\det(a_l * a_k, s * a_k)} = \frac{\det(a_l, p)}{\det(a_l, s)} = z_h^{(0)}, \\
z_g^{(0)} &= \frac{c\,\det(a_k, p)}{c\,\det(a_k, s * a_l)} = \frac{\det(a_l, p)}{\det(a_l, s * a_l)} = z_h^{(0)}.
\end{aligned}$$

If j is negative crossing, then by exchanging the indices $e \leftrightarrow g$ in the above calculation, we obtain the same result.

Note that Lemma 2.4 and the definition of p in Section 2.3 guarantee $z_k^{(0)} \neq 0, 1, \infty$ and $(w_k^j)^{(0)} \neq 0, 1$, so we will concentrate on proving $(z_1^{(0)}, \ldots, z_n^{(0)}, (w_k^j)^{(0)}, \ldots) \in \mathcal{S}$.

Consider the positive crossing j in Figure 20(a) and assume it is non-degenerate. Also consider the tetrahedra in Figures 9(a) and 10(a), and assign variables z_e, z_f, z_g, z_h to sides of the link diagram as in Figure 20(a). Then, using (20) and (31), the shape parameters

assigned to the horizontal edges $\mathrm{A}_j\mathrm{B}_j$ and $\mathrm{D}_j\mathrm{A}_j$ are

$$\begin{aligned} 1 &\neq [h(s*a_k), h(p), h(\pm a_l * a_k), h(a_k)] \\ &= \frac{\det(s, a_k)}{\det(s*a_k, \pm a_l * a_k)} \frac{\det(p, \pm a_l * a_k)}{\det(p, a_k)} = \frac{z_f^{(0)}}{z_e^{(0)}}, \\ 1 &\neq [h(s), h(p), h(a_k), h(a_l)] = \frac{\det(s, a_l)}{\det(s, a_k)} \frac{\det(p, a_k)}{\det(p, a_l)} = \frac{z_e^{(0)}}{z_h^{(0)}}, \end{aligned}$$

respectively. Likewise, the shape parameters assigned to $\mathrm{B}_j\mathrm{C}_j$ and $\mathrm{C}_j\mathrm{D}_j$ are $\frac{z_g^{(0)}}{z_f^{(0)}}$ and $\frac{z_h^{(0)}}{z_g^{(0)}}$ respectively. Furthermore, for any $a, b \in \mathbb{C}^2 \backslash \{0\}$, we can easily show that $h(a*b-a) = h(b)$. If $\frac{z_g^{(0)}}{z_e^{(0)}} = \frac{\det(a_k, s)}{\det(a_k, s*a_l)} = 1$, then $h(a_k) = h(s*a_l - s) = h(a_l)$, which is contradiction. Therefore, we obtain $\frac{z_g^{(0)}}{z_e^{(0)}} \neq 1$, and $\frac{z_h^{(0)}}{z_f^{(0)}} \neq 1$ can be obtained similarly.

We can verify the same holds for non-degenerate negative crossing j by the same way.

Now consider the case when the positive crossing j in Figure 20(a) is degenerate. (See Figures 7(c) and 11(a).) Then, using (20) and (32), the shape parameters assigned to the edges $\mathrm{F}_j\mathrm{A}_j$, $\mathrm{E}_j\mathrm{B}_j$, $\mathrm{F}_j\mathrm{C}_j$ and $\mathrm{E}_j\mathrm{D}_j$ in Figure 7(c) are

$$\begin{aligned} [h(a_k), h(s), h(p), h(s*a_l)][h(a_k), h(s*a_k), h((s*a_l)*a_k), h(p)] \\ = \frac{\det(s, p)}{\det(s*a_k, p)} = (w_e^j)^{(0)}, \\ [h(\pm a_l * a_k), h(p), h((s*a_l)*a_k), h(s*a_k)] \\ = \frac{\det(p, (s*a_l)*a_k)}{\det(p, s*a_k)} = (w_f^j)^{(0)}, \\ [h(a_k), h((s*a_l)*a_k), h(p), h(s*a_k)][h(a_k), h(s*a_l), h(s), h(p)] \\ = \frac{\det((s*a_l)*a_k, p)}{\det(s*a_l, p)} = (w_g^j)^{(0)}, \\ [h(a_l), h(p), h(s), h(s*a_l)] \\ = \frac{\det(p, s)}{\det(p, s*a_l)} = (w_h^j)^{(0)}, \end{aligned}$$

respectively. We can verify the same holds for degenerate negative crossing j by the same way.

Therefore $(z_1^{(0)}, \ldots, z_n^{(0)}, (w_k^j)^{(0)}, \ldots)$ satisfies the hyperbolicity equations of octahedral triangulation defined in Section 2.3 and, from Proposition 3.1, we obtain $(z_1^{(0)}, \ldots, z_n^{(0)}, (w_k^j)^{(0)}, \ldots)$ is a solution of $\mathcal{H}$. By the definition of $\mathcal{S}$, we obtain $(z_1^{(0)}, \ldots, z_n^{(0)}, (w_k^j)^{(0)}, \ldots) \in \mathcal{S}$.

□

To obtain the complex volume of ρ from the potential function $V(z_1, \ldots, z_n, (w_k^j), \ldots)$, we

modify it to

$$V_0(z_1,\dots,z_n,(w_k^j),\dots) := V(z_1,\dots,z_n,(w_k^j),\dots) \\ -\sum_k \left(z_k\frac{\partial V}{\partial z_k}\right)\log z_k - \sum_{\substack{j:\text{degenerate}\\ k}} \left(w_k^j\frac{\partial V}{\partial w_k^j}\right)\log w_k^j. \tag{33}$$

This modification guarantees the invariance of the value under the choice of any log-branch. (See Lemma 2.1 of [4].) Note that $V_0(z_1^{(0)},\dots,z_n^{(0)},(w_k^j)^{(0)},\dots)$ means the evaluation of the function $V_0(z_1,\dots,z_n,(w_k^j),\dots)$ at $(z_1^{(0)},\dots,z_n^{(0)},(w_k^j)^{(0)},\dots)$.

Theorem 3.3. *Consider a hyperbolic link L, the shadow-coloring induced by ρ, the potential function $V(z_1,\dots,z_n,(w_k^j),\dots)$ and the solution $(z_1^{(0)},\dots,z_n^{(0)},(w_k^j)^{(0)},\dots) \in \mathcal{S}$ defined in Theorem 3.2. Then,*

$$V_0(z_1^{(0)},\dots,z_n^{(0)},(w_k^j)^{(0)},\dots) \equiv i(\mathrm{vol}(\rho)+i\,\mathrm{cs}(\rho)) \pmod{\pi^2}. \tag{34}$$

Proof. When the crossing j is degenerate, direct calculation shows that the potential function V_j of the crossing defined at (27) satisfies

$$(V_j)_0(z,z,z,z,w_1,w_2,w_3) = 0, \tag{35}$$

for any nonzero values of z, w_1, w_2, w_3. To simplify the potential function, we rearrange the side variables $z_1,\dots,z_n$ to $z_1,\dots,z_r$, $z_{r+1}, z_{r+1}^1, z_{r+1}^2, z_{r+1}^3, \dots, z_t,\dots,z_t^3$ so that all endpoints of sides with variables $z_1,\dots,z_r$ are non-degenerate crossings and the degenerate crossings induce $z_{r+1}^{(0)} = (z_{r+1}^1)^{(0)} = (z_{r+1}^2)^{(0)} = (z_{r+1}^3)^{(0)}$, …, $z_t^{(0)} = \dots = (z_t^3)^{(0)}$. (Refer (32).) Then we define simplified potential function $\widehat{V}$ by

$$\widehat{V}(z_1,\dots,z_t) := \sum_{j:\text{non-degenerate}} V_j(z_1,\dots,z_r,z_{r+1},z_{r+1},z_{r+1},z_{r+1},\dots,z_t,z_t,z_t,z_t).$$

Note that $\widehat{V}$ is obtained from V by removing the potential functions (27) of the degenerate crossings and substituting the side variables z_e, z_f, z_g, z_h around the degenerate crossing with z_e. From (35), we have

$$\widehat{V}_0(z_1^{(0)},\dots,z_t^{(0)}) = V_0(z_1^{(0)},\dots,z_n^{(0)},(w_k^j)^{(0)},\dots),$$

which suggests $\widehat{V}$ is just a simplification of V with the same value. Therefore, from now on, we will use only $\widehat{V}$ and substitute the side variables of the link diagram $z_{r+1}^1, z_{r+1}^2, z_{r+1}^3$ to z_{r+1} and $z_t^1,\dots,z_t^3$ to z_t, etc, except at Lemma 3.4 below. Also, we remove octahedra (14) or (15) placed at all degenerate crossings (in other words, the octahedra in Figure 10) because they do not have any effect on the complex volume. (See the comment below the proof of Theorem 2.10.)

Now we will follow ideas of the proof of Theorem 1.2 in [4]. However, due to the degenerate crossings, we will improve the proof to cover more general cases. At first, we define r_k by

$$r_k \pi i = z_k \frac{\partial \widehat{V}}{\partial z_k}\bigg|_{z_1=z_1^{(0)},\ldots,z_t=z_t^{(0)}}, \tag{36}$$

for $k = 1, \ldots, t$, where $|_{z_1=z_1^{(0)},\ldots,z_t=z_t^{(0)}}$ means the evaluation of the equation at $(z_1^{(0)}, \ldots, z_t^{(0)})$. Unlike [4], we cannot guarantee r_k is an even integer yet, so we need the following lemma.

Lemma 3.4. *For the value $z_k^{(0)}$ defined in Theorem 3.2, $(z_1^{(0)}, \ldots, z_t^{(0)})$ is a solution of the following set of equations*

$$\widehat{\mathcal{H}} = \left\{ \exp(z_k \frac{\partial \widehat{V}}{\partial z_k}) = 1 \;\middle|\; k = 1, \ldots, t \right\}.$$

Proof. For a degenerate crossing j, from (27),

$$V_j(z_k, z_k, z_k, z_k, w_e^j, w_f^j, w_g^j) = (-\log w_e^j + \log w_f^j - \log w_g^j + \log w_h^j) \log z_k.$$

Therefore, using $\frac{w_f^j w_h^j}{w_e^j w_g^j} = 1$, we obtain

$$\exp\left(z_k \frac{\partial V_j}{\partial z_k}(z_k, z_k, z_k, z_k, w_e^j, w_f^j, w_g^j) \right) = 1.$$

This equation implies that, if we substitute the variables $z_{r+1}^1, z_{r+1}^2, z_{r+1}^3$ to z_{r+1} and $z_t^1, \ldots, z_t^3$ to z_t, etc, of the equations in $\mathcal{H}$, then it becomes $\widehat{\mathcal{H}}$. Therefore, Theorem 3.2 induces this lemma.

□

As a corollary of Lemma 3.4, now we know r_k defined in (36) is an even integer.

To avoid redundant complicate indices, we use z_k instead of $z_k^{(0)}$ in this proof from now on. Using the even integer r_k, we can denote $V_0(z_1, \ldots, z_t)$ by

$$\widehat{V_0}(z_1, \ldots, z_t) = \widehat{V}(z_1, \ldots, z_t) - \sum_{k=1}^{t} r_k \pi i \log z_k. \tag{37}$$

Now we introduce notations $\alpha_m, \beta_m, \gamma_l, \delta_j$ for the long-edge parameters defined in (19). We assign α_m and β_m to non-horizontal edges as in Figure 21, where m is over all sides of the link diagram. (Recall that the edges $\mathrm{A}_j\mathrm{B}_j$, $\mathrm{B}_j\mathrm{C}_j$, $\mathrm{C}_j\mathrm{D}_j$ and $\mathrm{D}_j\mathrm{A}_j$ in Figure 21 were named horizontal edges.) We also assign γ_l to horizontal edges, where l is over all regions, and δ_j to the edge $\mathrm{E}_j\mathrm{F}_j$ inside the octahedron. Although we have $\alpha_a = \alpha_c$ and $\beta_b = \beta_d$ because of the gluing, we use α_a for the tetrahedron $\mathrm{E}_j\mathrm{F}_j\mathrm{A}_j\mathrm{B}_j$ and $\mathrm{E}_j\mathrm{F}_j\mathrm{A}_j\mathrm{D}_j$, α_c for $\mathrm{E}_j\mathrm{F}_j\mathrm{C}_j\mathrm{B}_j$ and $\mathrm{E}_j\mathrm{F}_j\mathrm{C}_j\mathrm{D}_j$, β_b for $\mathrm{E}_j\mathrm{F}_j\mathrm{A}_j\mathrm{B}_j$ and $\mathrm{E}_j\mathrm{F}_j\mathrm{C}_j\mathrm{B}_j$, β_d for $\mathrm{E}_j\mathrm{F}_j\mathrm{C}_j\mathrm{D}_j$ and $\mathrm{E}_j\mathrm{F}_j\mathrm{A}_j\mathrm{D}_j$, respectively.

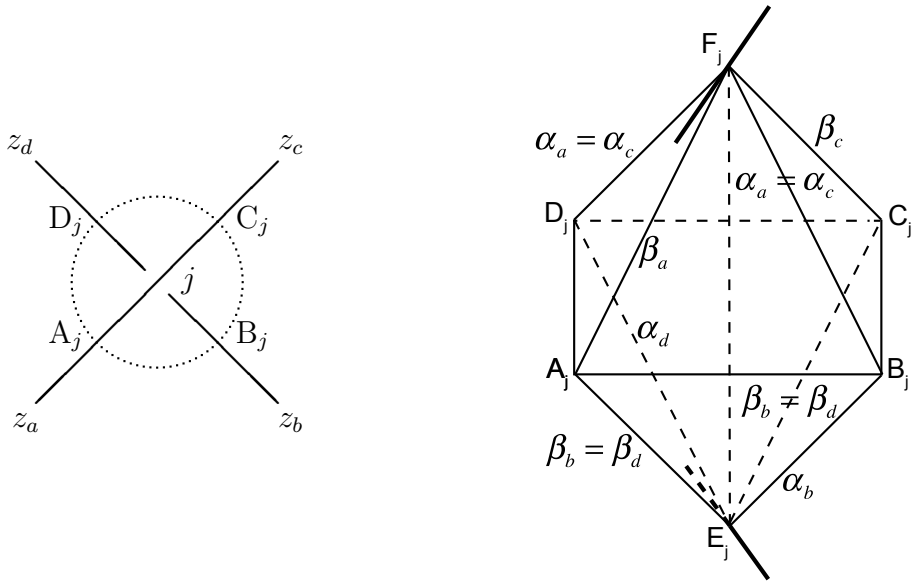

Figure 21: Long-edge parameters of non-horizontal edges

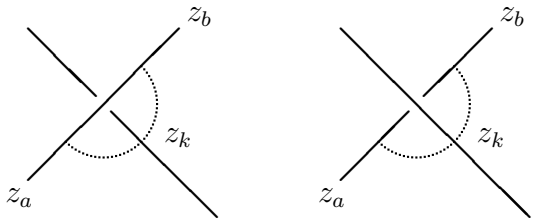

Figure 22: Two cases with respect to z_k

Note that the labeling is consistent even when some crossing is degenerate because, when the crossing j in Figure 21 is degenerate, we obtain $z_a = z_b = z_c = z_d$ and, after removing the octahedron of the crossing, the long-edge parameters satisfy $\alpha_a = \alpha_b = \alpha_c = \alpha_d$ and $\beta_a = \beta_b = \beta_c = \beta_d$.

Now consider a side with variable z_k and two possible cases in Figure 22. We consider the case when the crossing is non-degenerate, or equivalently, $z_a \neq z_k \neq z_b$. (If it is degenerate, we assume there is a degenerated octahedron[10] at the crossing.) For $m = a, b$, let $\sigma_k^m \in \{\pm 1\}$ be the sign of the tetrahedron[11] between the sides z_k and z_m, and u_k^m be the shape parameter of the tetrahedron assigned to the horizontal edge. We put $\tau_k^m = 1$ when z_k is the numerator of $(u_k^m)^{\sigma_k^m}$ and $\tau_k^m = -1$ otherwise. We also define p_k^m and q_k^m by (24) so that $\sigma_k^m[(u_k^m)^{\sigma_k^m}; p_k^m, q_k^m]$ becomes the element of $\widehat{\mathcal{P}}(\mathbb{C})$ corresponding to the tetrahedron.

[10] Octahedron is called degenerate when two vertices at the top and the bottom coincide.

[11] Sign of a tetrahedron is the sign of the coordinate in (12) or (13).

Then $\frac{1}{2}\sum_{1\le k,m\le t}\sigma_k^m[(u_k^m)^{\sigma_k^m};p_k^m,q_k^m]$ is the element[12] of $\widehat{\mathcal{B}}(\mathbb{C})$ corresponding to the octahedral triangulation in Section 2.3, and

$$\frac{1}{2}\sum_{1\le k,m\le t}\sigma_k^m\widehat{L}[(u_k^m)^{\sigma_k^m};p_k^m,q_k^m]\equiv i(\mathrm{vol}(\rho)+i\,\mathrm{cs}(\rho))\pmod{\pi^2}, \tag{38}$$

from Theorem 2.10.

By definition, we know

$$u_k^a=\frac{z_k}{z_a},\ u_k^b=\frac{z_b}{z_k}. \tag{39}$$

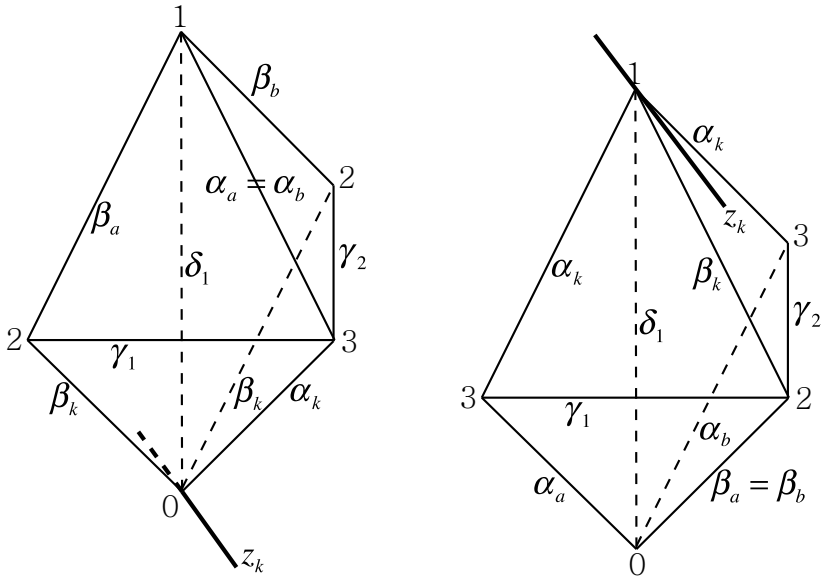

Figure 23: Tetrahedra of Figure 22

In the case of Figure 22(a), we have

$$\sigma_k^a=1,\ \sigma_k^b=-1\ \text{ and }\ \tau_k^a=\tau_k^b=1.$$

Using the equation (24) and Figure 23(a), we decide p_k^m and q_k^m as follows:

$$\begin{cases}\log\frac{z_k}{z_a}+p_k^a\pi i=(\log\alpha_k-\log\beta_k)-(\log\alpha_a-\log\beta_a),\\ \log\frac{z_k}{z_b}+p_k^b\pi i=(\log\alpha_k-\log\beta_k)-(\log\alpha_b-\log\beta_b),\end{cases} \tag{40}$$

$$\begin{cases}-\log(1-\frac{z_k}{z_a})+q_k^a\pi i=\log\beta_k+\log\alpha_a-\log\gamma_1-\log\delta_1,\\ -\log(1-\frac{z_k}{z_b})+q_k^b\pi i=\log\beta_k+\log\alpha_b-\log\gamma_2-\log\delta_1.\end{cases} \tag{41}$$

[12] The coefficient $\frac{1}{2}$ appears because the same tetrahedron is counted twice in the summation.

In the case of Figure 22(b), we have

$$\sigma_k^a = -1,\ \sigma_k^b = 1 \ \text{ and } \ \tau_k^a = \tau_k^b = -1.$$

Using the equation (24) and Figure 23(b), we decide p_k^m and q_k^m as follows:

$$\begin{cases} \log \frac{z_a}{z_k} + p_k^a \pi i = (\log \alpha_a - \log \beta_a) - (\log \alpha_k - \log \beta_k), \\ \log \frac{z_b}{z_k} + p_k^b \pi i = (\log \alpha_b - \log \beta_b) - (\log \alpha_k - \log \beta_k), \end{cases} \tag{42}$$

$$\begin{cases} -\log(1 - \frac{z_a}{z_k}) + q_k^a \pi i = \log \beta_a + \log \alpha_k - \log \gamma_1 - \log \delta_1, \\ -\log(1 - \frac{z_b}{z_k}) + q_k^b \pi i = \log \beta_b + \log \alpha_k - \log \gamma_2 - \log \delta_1. \end{cases} \tag{43}$$

The equations (40) and (42) holds for all (non-degenerate and degenerate) crossings, so we get the following observation.

Observation 3.5. *We have*

$$\log \alpha_k - \log \beta_k \equiv \log z_k + A \pmod{\pi i},$$

for all $k = 1, \ldots, t$, where A is a complex constant number independent of k.

Note that, by the definition (26), the potential function $\widehat{V}$ is expressed by

$$\widehat{V}(z_1, \ldots, z_t) = \frac{1}{2} \sum_{1 \le k, m \le t} \sigma_k^m \mathrm{Li}_2((u_k^m)^{\sigma_k^m}) = \frac{1}{2} \sum_{k=1}^{t} \sum_{m=a,\ldots,d} \sigma_k^m \mathrm{Li}_2((u_k^m)^{\sigma_k^m}), \tag{44}$$

where the range of the index m is determined by k and we put the range of m by $m = a, \ldots, d$[13] from now on. Recall that r_k was defined in (36). Direct calculation shows

$$r_k \pi i = -\sum_{m=a,\ldots,d} \sigma_k^m \tau_k^m \log(1 - (u_k^m)^{\sigma_k^m}).$$

Combining (41) and (43), we obtain

$$\sum_{m=a,b} \sigma_k^m \tau_k^m \left\{ -\log(1 - (u_k^m)^{\sigma_k^m}) + q_k^m \pi i \right\} = -\log \gamma_1 + \log \gamma_2,$$

for both cases in Figure 22. (Note that $\alpha_a = \alpha_b$ in (41) and $\beta_a = \beta_b$ in (43).) Therefore, we obtain

$$\sum_{m=a,\ldots,d} \sigma_k^m \tau_k^m \left\{ -\log(1 - (u_k^m)^{\sigma_k^m}) + q_k^m \pi i \right\} = 0,$$

and

$$r_k \pi i = -\sum_{m=a,\ldots,d} \sigma_k^m \tau_k^m q_k^m \pi i. \tag{45}$$

[13] The range $m = a, \ldots, d$ means that each side with one of the side variables $z_a, \ldots, z_d$ share a non-degenerate crossing with a side with z_k.

Lemma 3.6. *For all possible k and m, we have*

$$\frac{1}{2}\sum_{1\le k,m\le t}\sigma_k^m q_k^m \pi i \log(u_k^m)^{\sigma_k^m} \equiv -\sum_{k=1}^{t} r_k \pi i \log z_k \pmod{2\pi^2}. \tag{46}$$

Proof. Note that, by definition, $\sigma_k^m = \sigma_m^k$, $\tau_k^m = -\tau_m^k$ and

$$(u_k^m)^{\sigma_k^m} = \left(\frac{z_k}{z_m}\right)^{\tau_k^m} = (z_k)^{\tau_k^m}(z_m)^{\tau_m^k}.$$

Using the above and (45), we can directly calculate

$$\begin{aligned}\frac{1}{2}\sum_{k=1}^{t}\sum_{m=a,\dots,d}\sigma_k^m q_k^m \pi i \log(u_k^m)^{\sigma_k^m} &\equiv \sum_{k=1}^{t}\left(\sum_{m=a,\dots,d}\sigma_k^m\tau_k^m q_k^m \pi i\right)\log z_k \pmod{2\pi^2}\\ &= -\sum_{k=1}^{t} r_k \pi i \log z_k.\end{aligned}$$

□

Lemma 3.7. *For all possible k and m, we have*

$$\frac{1}{2}\sum_{1\le k,m\le t}\sigma_k^m \log\left(1-(u_k^m)^{\sigma_k^m}\right)\left(\log(u_k^m)^{\sigma_k^m} + p_k^m \pi i\right) \equiv -\sum_{k=1}^{t} r_k \pi i \log z_l \pmod{2\pi^2}.$$

Proof. From (40) and (42), we have

$$\log(u_k^m)^{\sigma_k^m} + p_k^m \pi i = \tau_k^m(\log\alpha_k - \log\beta_k) + \tau_m^k(\log\alpha_m - \log\beta_m).$$

Therefore,

$$\begin{aligned}&\frac{1}{2}\sum_{1\le k,m\le t}\sigma_k^m \log\left(1-(u_k^m)^{\sigma_k^m}\right)\left(\log(u_k^m)^{\sigma_k^m} + p_k^m \pi i\right)\\ &\quad= \sum_{k=1}^{t}\left(\sum_{m=a,\dots,d}\sigma_k^m\tau_k^m \log(1-(u_k^m)^{\sigma_k^m})\right)(\log\alpha_k - \log\beta_k)\\ &\quad= -\sum_{k=1}^{t} r_k \pi i(\log\alpha_k - \log\beta_k).\end{aligned}$$

Note that

$$\sum_{k=1}^{t} r_k \pi i = \sum_{k=1}^{t} z_k \frac{\partial \widehat{V}}{\partial z_k} = 0$$

because $\widehat{V}$ is expressed by the summation of certain forms of $\mathrm{Li}_2(\frac{z_a}{z_b})$ and

$$z_a\frac{\partial \mathrm{Li}_2(z_a/z_b)}{\partial z_a}+z_b\frac{\partial \mathrm{Li}_2(z_a/z_b)}{\partial z_b}=-\log(1-\frac{z_a}{z_b})+\log(1-\frac{z_a}{z_b})=0.$$

By using Observation 3.5, the above and the fact that r_k is even, we have

$$-\sum_{k=1}^{t} r_k\pi i(\log\alpha_k-\log\beta_k)\equiv-\sum_{k=1}^{t} r_k\pi i(\log z_k+A)=-\sum_{k=1}^{t} r_k\pi i\log z_k \pmod{2\pi^2}.$$

□

Combining (38), (44), Lemma 3.6 and Lemma 3.7, we complete the proof of Theorem 3.3 as follows:

$$\begin{aligned} i(\mathrm{vol}(\rho)+i\,\mathrm{cs}(\rho)) &\equiv \frac{1}{2}\sum_{1\le k,m\le t}\sigma_k^m\widehat{L}[(u_k^m)^{\sigma_k^m};p_k^m,q_k^m]\\ &=\frac{1}{2}\sum_{1\le k,m\le t}\sigma_k^m\left(\mathrm{Li}_2\left((u_k^m)^{\sigma_k^m}\right)-\frac{\pi^2}{6}\right)+\frac{1}{4}\sum_{1\le k,m\le t}\sigma_k^m q_k^m\pi i\log\left(u_k^m\right)^{\sigma_k^m}\\ &\quad+\frac{1}{4}\sum_{1\le k,m\le t}\sigma_k^m\log\left(1-(u_k^m)^{\sigma_k^m}\right)\left(\log\left(u_k^m\right)^{\sigma_k^m}+p_k^m\pi i\right)\\ &\equiv\widehat{V}(z_1,\dots,z_n)-\sum_{k=1}^{t} r_k\pi i\log z_k=\widehat{V}_0(z_1,\dots,z_t) \pmod{\pi^2}. \end{aligned}$$

□

4 Examples

4.1 Figure-eight knot 4_1

For the figure-eight knot diagram in Figure 24, let the elements of $\mathcal{P}$ corresponding to the arcs be

$$a_1=\begin{pmatrix}0\\t\end{pmatrix},\ a_2=\begin{pmatrix}1\\0\end{pmatrix},\ a_3=\begin{pmatrix}-t\\1+t\end{pmatrix},\ a_4=\begin{pmatrix}-t\\t\end{pmatrix},$$

where t is a solution of $t^2+t+1=0$. These elements satisfy

$$a_1*a_2=a_4,\ a_3*a_4=a_2,\ a_1*a_3=-a_2,\ a_3*a_1=a_4, \tag{47}$$

where the identities are expressed in $\mathbb{C}^2\backslash\{0\}$, not in $\mathcal{P}=(\mathbb{C}^2\backslash\{0\})/\pm$. Let $\rho:\pi_1(4_1)\to\mathrm{PSL}(2,\mathbb{C})$ be the boundary-parabolic representation determined by $a_1,\dots,a_4$. We define the shadow-coloring of Figure 24 induced by ρ by letting

$$s_1=\begin{pmatrix}1\\1\end{pmatrix},\ s_2=\begin{pmatrix}0\\1\end{pmatrix},\ s_3=\begin{pmatrix}-t-1\\t+2\end{pmatrix},\ s_4=\begin{pmatrix}-2t-1\\2t+3\end{pmatrix},$$
$$s_5=\begin{pmatrix}-2t-1\\t+4\end{pmatrix},\ s_6=\begin{pmatrix}1\\t+2\end{pmatrix},\ p=\begin{pmatrix}2\\1\end{pmatrix}.$$

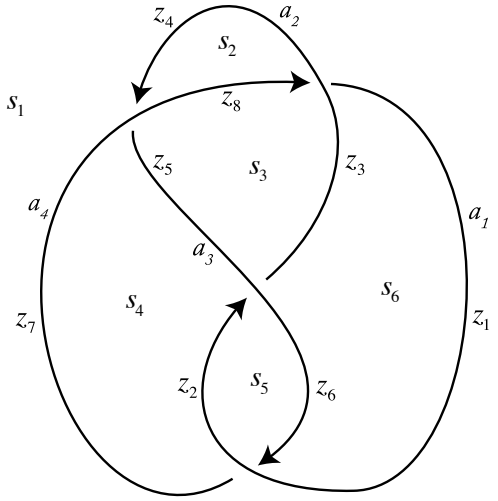

Figure 24: Figure-eight knot 4_1 with parameters

Direct calculation shows this shadow-coloring satisfies (4) in Lemma 2.4. (However, this does not satisfy (5).)

All values of $h(a_1), \ldots, h(a_4)$ are different, hence the potential function $V(z_1, \ldots, z_8)$ of Figure 24 is (28). Applying Theorem 3.2, we obtain

$$z_1^{(0)} = \frac{\det(a_1, p)}{\det(a_1, s_6)} = 2,\ z_2^{(0)} = \frac{\det(a_1, p)}{\det(a_1, s_5)} = \frac{-2}{2t+1},\ z_3^{(0)} = \frac{\det(a_2, p)}{\det(a_2, s_6)} = \frac{1}{t+2},$$
$$z_4^{(0)} = \frac{\det(a_2, p)}{\det(a_2, s_1)} = 1,\ z_5^{(0)} = \frac{\det(a_3, p)}{\det(a_3, s_4)} = -3t-2,\ z_6^{(0)} = \frac{\det(a_3, p)}{\det(a_3, s_5)} = \frac{3t+2}{2t},$$
$$z_7^{(0)} = \frac{\det(a_4, p)}{\det(a_4, s_4)} = \frac{3}{2},\ z_8^{(0)} = \frac{\det(a_4, p)}{\det(a_4, s_3)} = 3,$$

and $(z_1^{(0)}, \ldots, z_8^{(0)})$ becomes a solution of $\mathcal{H} = \{\exp(z_k \frac{\partial V}{\partial z_k}) = 1 \mid k = 1, \ldots, 8\}$. Applying Theorem 3.3, we obtain

$$V_0(z_1^{(0)}, \ldots, z_8^{(0)}) \equiv i(\mathrm{vol}(\rho) + i\,\mathrm{cs}(\rho)) \pmod{\pi^2},$$

and numerical calculation verifies it by

$$V_0(z_1^{(0)}, \ldots, z_8^{(0)}) = \begin{cases} i(2.0299... + 0\,i) = i(\mathrm{vol}(4_1) + i\,\mathrm{cs}(4_1)) & \text{if } t = \frac{-1-\sqrt{3}\,i}{2}, \\ i(-2.0299... + 0\,i) = i(-\mathrm{vol}(4_1) + i\,\mathrm{cs}(4_1)) & \text{if } t = \frac{-1+\sqrt{3}\,i}{2}. \end{cases}$$

4.2 Trefoil knot 3_1

For the trefoil knot diagram in Figure 25, let the elements of $\mathcal{P}$ corresponding to the arcs be

$$a_1 = \begin{pmatrix} 1 \\ 0 \end{pmatrix},\ a_2 = \begin{pmatrix} 0 \\ 1 \end{pmatrix},\ a_3 = a_4 = \begin{pmatrix} -1 \\ 1 \end{pmatrix}.$$

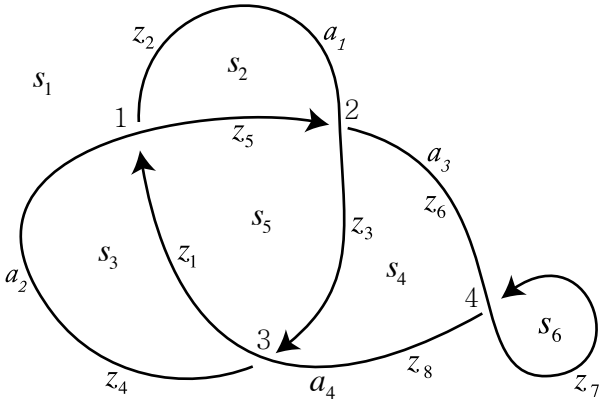

Figure 25: Trefoil knot 3_1 with parameters

(Note that crossing 4 is degenerate.) These elements satisfy

$$a_4 * a_2 = -a_1,\ a_2 * a_1 = a_3,\ a_1 * a_4 = a_2,\ a_4 * a_3 = a_3. \tag{48}$$

where the identities are expressed in $\mathbb{C}^2\backslash\{0\}$, not in $\mathcal{P} = (\mathbb{C}^2\backslash\{0\})/\pm$. Let $\rho : \pi_1(3_1) \to \mathrm{PSL}(2,\mathbb{C})$ be the boundary-parabolic representation determined by a_1, a_2, a_3, a_4. We define the shadow-coloring of Figure 24 induced by ρ by letting

$$s_1 = \begin{pmatrix} -1 \\ 2 \end{pmatrix},\ s_2 = \begin{pmatrix} 1 \\ 2 \end{pmatrix},\ s_3 = \begin{pmatrix} -1 \\ 3 \end{pmatrix},\ s_4 = \begin{pmatrix} 0 \\ 1 \end{pmatrix},$$
$$s_5 = \begin{pmatrix} 1 \\ 1 \end{pmatrix}, s_6 = \begin{pmatrix} -2 \\ 3 \end{pmatrix},\ p = \begin{pmatrix} 2 \\ 1 \end{pmatrix}.$$

Direct calculation shows this shadow-coloring satisfies (4) in Lemma 2.4. (However, this does not satisfy (5).)

All values of $h(a_1), h(a_2), h(a_3) = h(a_4)$ are different, hence the potential function V of Figure 25 is

$$\begin{aligned} V(z_1,\dots,z_8,w_6^4,w_7^4) &= \mathrm{Li}_2(\frac{z_2}{z_5}) - \mathrm{Li}_2(\frac{z_2}{z_4}) + \mathrm{Li}_2(\frac{z_1}{z_4}) - \mathrm{Li}_2(\frac{z_1}{z_5}) \\ &+ \mathrm{Li}_2(\frac{z_6}{z_3}) - \mathrm{Li}_2(\frac{z_6}{z_2}) + \mathrm{Li}_2(\frac{z_5}{z_2}) - \mathrm{Li}_2(\frac{z_5}{z_3}) \\ &+ \mathrm{Li}_2(\frac{z_4}{z_1}) - \mathrm{Li}_2(\frac{z_4}{z_8}) + \mathrm{Li}_2(\frac{z_3}{z_8}) - \mathrm{Li}_2(\frac{z_3}{z_1}) \\ &- \log w_6^4 \log z_6 + \log w_6^4 \log z_8, \end{aligned}$$

and the simplified potential function $\widehat{V}$ defined in the proof of Theorem 3.3 is

$$\begin{aligned} \widehat{V}(z_1,\dots,z_6) &= \mathrm{Li}_2(\frac{z_2}{z_5}) - \mathrm{Li}_2(\frac{z_2}{z_4}) + \mathrm{Li}_2(\frac{z_1}{z_4}) - \mathrm{Li}_2(\frac{z_1}{z_5}) \\ &+ \mathrm{Li}_2(\frac{z_6}{z_3}) - \mathrm{Li}_2(\frac{z_6}{z_2}) + \mathrm{Li}_2(\frac{z_5}{z_2}) - \mathrm{Li}_2(\frac{z_5}{z_3}) \\ &+ \mathrm{Li}_2(\frac{z_4}{z_1}) - \mathrm{Li}_2(\frac{z_4}{z_6}) + \mathrm{Li}_2(\frac{z_3}{z_6}) - \mathrm{Li}_2(\frac{z_3}{z_1}). \end{aligned}$$

Applying Theorem 3.2, we obtain

$$z_1^{(0)} = \frac{\det(a_4, p)}{\det(a_4, s_5)} = \frac{3}{2},\ z_2^{(0)} = \frac{\det(a_1, p)}{\det(a_1, s_2)} = \frac{1}{2},\ z_3^{(0)} = \frac{\det(a_1, p)}{\det(a_1, s_5)} = 1,$$
$$z_4^{(0)} = \frac{\det(a_2, p)}{\det(a_2, s_3)} = -2,,\ z_5^{(0)} = \frac{\det(a_2, p)}{\det(a_2, s_5)} = 2,$$
$$z_6^{(0)} = z_7^{(0)} = z_8^{(0)} = \frac{\det(a_3, p)}{\det(a_3, s_4)} = 3,$$
$$(w_6^4)^{(0)} = \frac{\det(s_1, p)}{\det(s_4, p)} = \frac{5}{2},\ (w_7^4)^{(0)} = \frac{\det(s_1, p)}{\det(s_6, p)} = \frac{5}{8}.$$

Note that $(z_1^{(0)}, \ldots, z_8^{(0)}, (w_6^4)^{(0)}, (w_7^4)^{(0)})$ and $(z_1^{(0)}, \ldots, z_6^{(0)})$ are solutions of

$$\mathcal{H} = \left\{ \exp(z_k \frac{\partial V}{\partial z_k}) = 1,\ \exp(w_k^j \frac{\partial V}{\partial w_k^j}) = 1 \mid j = 4,\ k = 1, \ldots, 8 \right\}$$
$$\text{and } \widehat{\mathcal{H}} = \left\{ \exp(z_k \frac{\partial \widehat{V}}{\partial z_k}) = 1 \mid k = 1, \ldots, 6 \right\},$$

respectively. Applying Theorem 3.3, we obtain

$$V_0(z_1^{(0)}, \ldots, (w_7^4)^{(0)}) \equiv \widehat{V}_0(z_1^{(0)}, \ldots, z_6^{(0)}) \equiv i(\mathrm{vol}(\rho) + i\,\mathrm{cs}(\rho)) \pmod{\pi^2},$$

and numerical calculation verifies it by

$$\widehat{V}_0(z_1^{(0)}, \ldots, z_6^{(0)}) = i(0 + 1.6449...i),$$

where $\mathrm{vol}(3_1) = 0$ holds trivially and $1.6449... = \frac{\pi^2}{6}$ holds numerically.

Acknowledgments The author appreciates Yuichi Kabaya and Jun Murakami for suggesting this research and having much discussion. Ayumu Inoue gave wonderful lectures on his work [9] at Seoul National University and it became the framework of Section 2 of this article. Many people including Hyuk Kim, Seonhwa Kim, Roland van der Veen, Hitoshi Murakami, Satoshi Nawata, Stephané Baseilhac, and KIAS members, heard my talks on the result and gave many suggestions.

The author is supported by Basic Science Research Program through the National Research Foundation of Korea (NRF) funded by the Ministry of Education (2014047764 and NRF-2015R1C1A1A02037540).

References

[1] J. Cho. Optimistic limits of colored Jones polynomials and complex volumes of hyperbolic links. arXiv:1303.3701. To appear in J. Aust. Math. Soc., 03 2013.

[2] J. Cho. Optimistic limit of the colored Jones polynomial and the existence of a solution. arXiv:1410.0525. To appear in Proc. AMS., 10 2014.

[3] J. Cho. Connected sum of representations of knot groups. *J. Knot Theory Ramifications*, 24(3):1550020 (18 pages), 2015.

[4] J. Cho, H. Kim, and S. Kim. Optimistic limits of Kashaev invariants and complex volumes of hyperbolic links. *J. Knot Theory Ramifications*, 23(10):1450049 (32 pages), 2014.

[5] J. Cho and J. Murakami. Reidemeister transformations of the potential function and the solution. arXiv.org:1509.02378, 09 2015.

[6] M. Elhamdadi and S. Nelson. *Quandles—an introduction to the algebra of knots*, volume 74 of *Student Mathematical Library*. American Mathematical Society, Providence, RI, 2015.

[7] S. Garoufalidis, M. Goerner, and C. K. Zickert. The Ptolemy field of 3-manifold representations. *Algebr. Geom. Topol.*, 15(1):371–397, 2015.

[8] K. Hikami and R. Inoue. Braids, complex volume and cluster algebras. *Algebr. Geom. Topol.*, 15(4):2175–2194, 2015.

[9] A. Inoue and Y. Kabaya. Quandle homology and complex volume. *Geom. Dedicata*, 171:265–292, 2014.

[10] R. M. Kashaev. A link invariant from quantum dilogarithm. *Modern Phys. Lett. A*, 10(19):1409–1418, 1995.

[11] F. Luo, S. Tillmann, and T. Yang. Thurston's spinning construction and solutions to the hyperbolic gluing equations for closed hyperbolic 3-manifolds. *Proc. Amer. Math. Soc.*, 141(1):335–350, 2013.

[12] W. D. Neumann. Extended Bloch group and the Cheeger-Chern-Simons class. *Geom. Topol.*, 8:413–474 (electronic), 2004.

[13] D. Rolfsen. *Knots and links*, volume 7 of *Mathematics Lecture Series*. Publish or Perish, Inc., Houston, TX, 1990. Corrected reprint of the 1976 original.

[14] J. Weeks. Computation of hyperbolic structures in knot theory. In *Handbook of knot theory*, pages 461–480. Elsevier B. V., Amsterdam, 2005.

[15] C. K. Zickert. The volume and Chern-Simons invariant of a representation. *Duke Math. J.*, 150(3):489–532, 2009.

Pohang Mathematics Institute, POSTECH
Gyungbuk 37673
Republic of Korea E-mail: dol0425@gmail.com